Journal of the American Heart Association

ORIGINAL RESEARCH

Modeling the Progression of Cardiac Catecholamine Deficiency in Lewy Body Diseases

David S. Goldstein, MD, PhD; Mark J. Pekker, PhD;* Patti Sullivan, CMT; Risa Isonaka, PhD; Yehonatan Sharabi, MD

BACKGROUND: Lewy body diseases (LBDs) feature deficiency of the sympathetic neurotransmitter norepinephrine in the left ventricular myocardium and sympathetic intra-neuronal deposition of the protein alpha-synuclein (αS). LBDs therefore are autonomic synucleinopathies. Computational modeling has revealed multiple functional abnormalities in residual myocardial sympathetic noradrenergic nerves in LBDs, including decreased norepinephrine synthesis, vesicular storage, and recycling. We report an extended model that enables predictions about the progression of LBDs and effects of genetic predispositions and treatments on that progression.

METHODS AND RESULTS: The model combines cardiac sympathetic activation with autotoxicity mediated by the dopamine metabolite 3,4-dihydroxyphenylacetaldehyde. We tested the model by its ability to predict longitudinal empirical data based on cardiac sympathetic neuroimaging, effects of genetic variations related to particular intra-neuronal reactions, treatment by monoamine oxidase inhibition to decrease 3,4-dihydroxyphenylacetaldehyde production, and post-mortem myocardial tissue contents of catecholamines and αS. The new model generated a triphasic decline in myocardial norepinephrine content. This pattern was confirmed by empirical data from serial cardiac ^{18}F-dopamine positron emission tomographic scanning in patients with LBDs. The model also correctly predicted empirical data about effects of genetic variants and monoamine oxidase inhibition and about myocardial levels of catecholamines and αS.

CONCLUSIONS: The present computational model predicts a triphasic decline in myocardial norepinephrine content as LBDs progress. According to the model, disease-modifying interventions begun at the transition from the first to the second phase delay the onset of symptomatic disease. Computational modeling coupled with biomarkers of preclinical autonomic synucleinopathy may enable early detection and more effective treatment of LBDs.

Key Words: catecholaldehyde ■ catecholamine ■ computational modeling ■ DOPAL, Lewy body ■ norepinephrine ■ sympathetic nervous system

Lewy body diseases (LBDs) are a family of aging-related neurodegenerative disorders that have in common the occurrence of Lewy bodies (LBs), cytoplasmic inclusions found in particular types of brainstem neurons. LBs contain the protein alpha-synuclein (αS),[1] and LBDs are in a family of diseases termed synucleinopathies. In LBDs αS deposition occurs both in neuronal cell bodies and in nerve fibers (Lewy neurites).

LBDs Entail Catecholamine Deficiencies in the Brain and Heart

LBDs are also characterized by deficiencies of the catecholamines norepinephrine and dopamine. Dopamine depletion in the nigrostriatal system, especially in the putamen,[2] causes the movement disorder that defines the most well-known LBD, Parkinson disease (PD).

Correspondence to: David S. Goldstein, MD, PhD, Autonomic Medicine Section, CNP/DIR/NINDS/NIH, 9000 Rockville Pike MSC-1620, Building 10 Room 8N260, Bethesda, MD 20892-1620. Email: goldsteind@ninds.nih.gov

*Formerly Mark J. Friedman.

Supplemental Material for this article is available at https://www.ahajournals.org/doi/suppl/10.1161/JAHA.121.024411

For Sources of Funding and Disclosures, see page 13.

JAHA is available at: www.ahajournals.org/journal/jaha

CLINICAL PERSPECTIVE

What Is New?

- We present a computational model to predict the progression of cardiac norepinephrine deficiency in Lewy body diseases and effects of genetic predispositions and treatments on that progression; the model applies the concepts of homeostasis/allostasis and of catecholamine autotoxicity mediated by the catecholaldehyde 3,4-dihydroxyphenylacetaldehyde in cardiac sympathetic nerves.
- The model predicts triphasic loss of myocardial norepinephrine stores (Phase 1=homeostasis, Phase 2=dyshomeostasis, Phase 3=symptomatic advanced disease).
- Attenuated 3,4-dihydroxyphenylacetaldehyde production via decreased monoamine oxidase activity results in later onset of symptomatic disease, while attenuated 3,4-dihydroxyphenylacetaldehyde metabolism via decreased aldehyde dehydrogenase activity results in earlier onset of symptomatic disease.

What Are the Clinical Implications?

- Treatment targeting 3,4-dihydroxyphenylacetaldehyde production and effects that is initiated in symptomatic disease produces only transient benefit, whereas the same treatment initiated at the transition from homeostasis to dyshomeostasis substantially delays the onset of symptomatic disease.
- The results reinforce the need to identify biomarkers of preclinical disease, to maximize efficacy of disease-modifying treatment.

Nonstandard Abbreviations and Acronyms

^{18}F-DA	^{18}F-dopamine
^{18}F-DOPA	^{18}F-3,4-dihydroxyphenylalanine
ALDH	aldehyde dehydrogenase
cTnT	cardiac troponin T
DBH	dopamine-beta-hydroxylase
DHPG	3,4-dihydroxyphenylglycol
DOPAC	3,4-dihydroxyphenylacetic acid
DOPAL	3,4-dihydroxyphenylacetaldehyde
DOPALc	cytoplasmic 3,4-dihydroxyphenylacetaldehyde
DOPEGAL	3,4-dihydroxyphenylglycolaldehyde
kALDH	rate constant for aldehyde dehydrogenase
kALDH_DOPALc	rate constant for aldehyde dehydrogenase acting on cytoplasmic 3,4-dihydroxyphenylacetaldehyde
kAR_DOPEGALc	rate constant for aldehyde/aldose reductase acting on cytoplasmic 3,4-dihydroxyphenyl glycolaldehyde
kDBH	rate constant for dopamine-beta-hydroxylase
kDHPGc_Loss	rate constant for loss of cytoplasmic 3,4-dihydroxyphenylglycol
kDOPAc_Loss	rate constant for loss of cytoplasmic 3,4-dihydroxyphenylalanine
kDOPACc_Loss	rate constant for loss of cytoplasmic 3,4-dihydroxyphenylacetic acid
kLAAAD	rate constant for L-aromatic-amino-acid decarboxylase
kLeak_DA	rate constant for leakage of dopamine from vesicles into cytoplasm
kLeak_NE	rate constant for leakage of norepinephrine from vesicles into cytoplasm
kMAO_DA	rate constant for monoamine oxidase acting on cytoplasmic dopamine
kMAO_NE	rate constant for monoamine oxidase acting on cytoplasmic norepinephrine
kNE_Release	rate constant for release of vesicular norepinephrine
kNEe_Loss	rate constant for loss of extracellular fluid norepinephrine
kTH	rate constant for tyrosine hydroxylase
kTYR_Loss	rate constant for tyrosine loss
kTYR_Uptake	rate constant for tyrosine uptake
kU1	rate constant for neuronal uptake via the cell membrane norepinephrine transporter
kVMAT_DA	rate constant for vesicular uptake of cytoplasmic dopamine mediated by the vesicular monoamine transporter
kVMAT_NE	rate constant for vesicular uptake of cytoplasmic norepinephrine mediated by the vesicular monoamine transporter

LAAAD	L-aromatic-amino-acid decarboxylase
LBDs	Lewy body diseases
Log10_VR	log of vascular relaxation
MAO_DA	monoamine oxidase acting on cytoplasmic dopamine
mCi	milliCuries
nCi	nanoCuries
NEv	vesicular norepinephrine
PAF	pure autonomic failure
PD	Parkinson disease
PUT/OCC	putamen/occipital cortex ratio
SMA	alpha-smooth muscle actin
TH	tyrosine hydroxylase
VMAT2	type 2 vesicular monoamine transporter
VR	vascular relaxation
αS	alpha-synuclein

LBDs also feature profound cardiac catecholamine deficiency. This was first suspected by sympathetic neuroimaging demonstrating decreased left ventricular ^{18}F-dopamine (^{18}F-DA)-derived radioactivity by positron emission tomographic (PET) scanning in PD and the related LBD pure autonomic failure (PAF).[3] Post-mortem analyses have documented drastically reduced (by ≥90%) myocardial norepinephrine content in patients with LBDs compared with control subjects.[4]

Denervation Combined With Functional Abnormalities in Residual Sympathetic Nerves Explains the Cardiac Catecholamine Deficiency Attending LBDs

What underlies cardiac catecholamine deficiency in LBDs? A seemingly straightforward answer would be loss of cardiac sympathetic nerve fibers that contain dopamine and norepinephrine —ie, denervation. The extent of myocardial catecholamine depletion, however, is greater than can be accounted for by denervation alone. The disparity suggests that dysfunctions in residual neurons contribute to the neurotransmitter deficiencies.

In confirmation of this suggestion, application of a computational modeling approach to account for the main known steps in synthesis, storage, release, reuptake, and metabolism of catecholamines in cardiac sympathetic nerves (Figure 1) has revealed multiple specific, functional intra-neuronal abnormalities in LBDs.[5] These dysfunctions include decreased vesicular uptake of cytoplasmic catecholamines via the type 2 vesicular monoamine transporter (VMAT2); increased passive leakage from storage vesicles into the cytoplasm; decreased activities of the enzymes tyrosine hydroxylase (TH) and L-aromatic amino acid decarboxylase (LAAAD), which are required for the synthesis of dopamine and norepinephrine; and decreased neuronal norepinephrine recycling via the Uptake-1 process mediated by the cell membrane norepinephrine transporter. In vivo and post-mortem studies of patients with LBD have reported evidence for all these abnormalities.[6–8]

Modeling Disease Progression in LBDs

The published model[5] does not deal with the progression from the healthy to the diseased state, nor the effects of particular genetic variants or treatments on that progression. In PD, longitudinal neuroimaging studies have indicated an inverse exponential curve for striatal dopamine deficiency, with a rapid early decline followed by a slow late decline.[9] Based on this curvilinearity one would expect disease-modifying treatments to be more effective early than late in the disease.

During an even earlier phase, it seems likely that neurotransmitter stores are maintained within healthy narrow bounds (homeostasis). A key purpose of extending the original published model is to explore the transition from the relatively stable homeostatic phase (Phase 1) to the unstable phase (Phase 2) when there would be an escape from homeostasis (dyshomeostasis).

To explain this transition we invoked the "catecholaldehyde hypothesis."[10] The catecholaldehyde 3,4-dihydroxyphenylacetaldehyde (DOPAL), an obligate intermediate of dopamine metabolism, is produced continuously in the cytoplasm of catecholaminergic neurons (Figure 1). According to the catecholaldehyde hypothesis, DOPAL is an "autotoxin"[11] that can harm or destroy the neurons in which it is produced.[12] From the point of view of computational modeling as applied to processes in cardiac sympathetic nerves, an appealing aspect of the catecholaldehyde hypothesis is that DOPAL is known to interfere with key reactions in catecholaminergic cells, including TH,[13] LAAAD,[14] and trans-membrane catecholamine transport.[15]

How might DOPAL-induced autotoxicity be linked to αS deposition, which as noted above is a characteristic feature of LBDs? DOPAL potently oligomerizes, forms quinoprotein adducts with (quinonizes), and aggregates αS.[14] DOPAL-induced αS oligomers in turn exert a variety of potentially harmful effects, including interference with vesicular[7] and mitochondrial[16] functions, which may precipitate rapid neurodegeneration.

Testing the Model

We tested the model by its ability to predict empirical data about the course of catecholamine

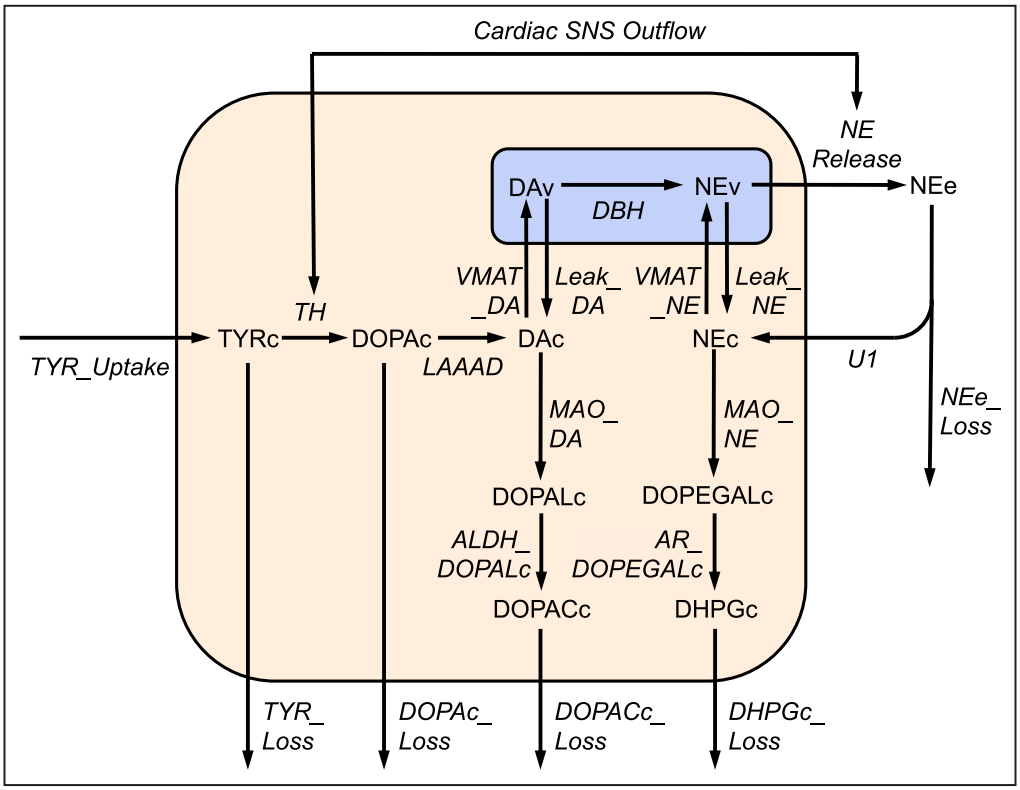

Figure 1. Pictorial representation of neuronal reactants and reactions in the computational model.

There are 11 reactants: (1) cytoplasmic tyrosine (TYRc), (2) cytoplasmic 3,4-dihydroxyphenylalanine (DOPAc), (3) cytoplasmic dopamine (DAc), (4) cytoplasmic 3,4-dihydroxyphenylacetic acid (DOPACc), (5) vesicular dopamine (DAv), (6) vesicular norepinephrine (NEv), (7) extracellular fluid norepinephrine (NEe), (8) cytoplasmic norepinephrine (NEc), (9) cytoplasmic 3,4-dihydroxyphenylglycol (DHPGc), (10) cytoplasmic 3,4-dihydroxyphenylacetaldehyde (DOPALc), and (11) cytoplasmic 3,4-dihydroxyphen ylglycolaldehyde (DOPEGALc). There are 19 reactions: (1) neuronal uptake of tyrosine (TYR_Uptake), (2) tyrosine loss from the neuron (TYR_Loss), (3) tyrosine hydroxylase (TH), (4) L-aromatic-amino-acid decarboxylase (LAAAD), (5) DOPA loss from the neuron (DOPAc_Loss), (6) vesicular leakage of vesicular dopamine (Leak_DA), (7) vesicular uptake of cytoplasmic dopamine (VMAT_DA), (8) monoamine oxidase acting on cytoplasmic dopamine (MAO_DA), (9) aldehyde dehydrogenase acting on DOPALc (ALDH_ DOPALc), (10) DOPAC loss from the neuron (DOPACc_Loss), (11) dopamine-beta-hydroxylase acting on vesicular dopamine (DBH), (12) vesicular uptake of cytoplasmic norepinephrine (VMAT_NE), (13) leakage of vesicular norepinephrine (Leak_NE), (14) exocytotic norepinephrine release (Norepinephrine Release), (15) neuronal uptake of extracellular fluid norepinephrine (U1) , (16) loss of extracellular fluid norepinephrine (NEe_Loss), (17) monoamine oxidase acting on cytoplasmic norepinephrine (MAO_NE), (18) aldehyde/ aldose reductase acting on cytoplasmic 3,4-dihydroxyphenylglycolaldehyde (AR_DOPEGALc), and (19) cytoplasmic 3,4-dihydroxyphenylglycol loss from the neuron (DHPGc_Loss). Homeostatic (reflexive) or allostatic (feed-forward) cardiac sympathetic noradrenergic system stimulation increases rate constant for release of vesicular norepinephrine (kNE_Release) and kTH.

deficiency in LBDs, effects of mutations of genes encoding enzymes or transporters in catecholaminergic neurons, results of preclinical and clinical testing of MAO inhibition, and post-mortem data about myocardial contents of catecholamines and αS in LBDs. These four aspects are described in more detail below.

Determining whether the model correctly predicts trends in norepinephrine stores requires a means to track myocardial norepinephrine content in living patients. For this we used cardiac sympathetic neuroimaging data. Cardiac ^{18}F-DA-derived radioactivity measured by positron emission tomography is correlated with post-mortem myocardial norepinephrine content.[17] Analogously, as an in vivo biomarker of nigrostriatal dopaminergic innervation we used the putamen/occipital cortex (PUT/OCC) ratio of 18F-3,4-dihydroxyphenylalanine (^{18}F-DOPA)-derived radioactivity.[18]

We tested the model by its ability to predict alterations in disease onset or progression because of hypofunctional variations in the genes encoding TH, LAAAD, VMAT2, the cell membrane norepinephrine

transporter, aldehyde dehydrogenase (ALDH, the main enzyme that detoxifies DOPAL), and MAO.

Since MAO inhibition would be expected to decrease DOPAL production and attenuate catecholaminergic neurodegeneration, we reviewed data from clinical trials about effects of MAO inhibitors on the symptomatic progression of PD.[19,20] We also explored whether combining MAO inhibition with treatment decreasing DOPAL effects would delay further the onset of symptomatic disease compared with MAO inhibition alone.

Finally, we examined whether predictions about αS buildup in sympathetic noradrenergic nerves fit with empirical post-mortem data about myocardial tissue contents of catecholamines and immunoreactive αS in the same specimens from patients with LBDs. With a view to extending to a potential in vivo biomarker, we also asked whether αS buildup in biopsiable scalp skin is associated with myocardial αS buildup and norepinephrine depletion in LBDs.

METHODS

The authors declare that all supporting data are available within the article online supplementary files.

Mathematical Underpinnings

The extended model is in the form of a system of 11 non-linear, parameterized, first-order ordinary differential equations that account for 25 reactions, including 19 intra-neuronal reactions (Figure 1, Tables S1 and S2). We investigated the model using the numerical continuation and bifurcation software CI_MatContL[21,22] (see Table S3 for code).

A stable equilibrium solution of this system accounts for a physiological state. A method for numerical investigation of such systems is numerical bifurcation analysis, which is based on continuation of solutions to well-defined operator equations. The equilibrium solutions are continued with respect to the input parameter, vascular relaxation (VR), which results in increased cardiac sympathetic outflow. A bifurcation signifies a sharp qualitative change in the solution when the continuation parameter changes only slightly. In the present model, an escape from or a breakdown of homeostasis occurs at the first Hopf bifurcation point, which results in a loss of stability and an onset of oscillations. Identifying such situations can mean acceleration of the disease process.

CI_MatCont is the command line MATLAB package for studying smaller-size dynamical systems and their bifurcations. CI_MatContL[22] is an extension of CI_MatCont to large-scale computations of bifurcations of equilibria via subspace reduction, based on the Continuation of Invariant Subspaces algorithm.[23] Key features of CI_MatContL include Continuation of Invariant Subspaces-based, continuous, well-scaled test functions for codimension 1 and 2 bifurcations, allowing accurate detection of bifurcations for large systems.

The models for the physiological processes under consideration are of the general form:

$$\dot{x}(t) = f(x(t), \alpha),$$

where x(t) is the state and α contains the parameter(s). A system exhibits homeostasis if some output variable remains constant, or almost constant, when an input variable or parameter changes by a relatively large amount. An example in autonomic medicine is cerebral autoregulation, in which cerebral blood flow is kept within a narrow range across blood pressures (BP). When we consider homeostasis defined as the output parameter being constant across a range of input parameters (Figure S1), homeostasis is a bifurcation of infinite codimension that can only be detected under special circumstances. The state x_0 at the output node(s) typically is not completely independent of the input parameter(s) α. The dependence there is more like a cubic function that is approximately constant in a certain range. This motivates the study of homeostasis in a local (infinitesimal) setting. For current mathematical models of mechanisms of homeostasis, we refer the reader to an article by Golubitsky et al[24] and references there.

When there is only one parameter α, infinitesimal homeostasis is observed at a point $\alpha = \alpha_0$ when $x_o'(\alpha_0) = 0$. Higher-order homeostasis cases occur when higher derivatives of $x_0(\alpha)$ vanish in a point. When there are multiple input parameters, the derivatives of x_0 with respect to all considered parameters are required to be zero at a homeostasis point. The type of homeostasis point is then characterized by the higher-order derivatives at the homeostasis point.

An example of a homeostasis point in a biological network with two input parameters is shown in Figure S1C.[25] Here extracellular dopamine varies depending on the activities of TH and the cell membrane dopamine transporter. There are several different types of homeostatic points for two input parameters that are characterized by the higher-order derivatives of x_0. A healthy state corresponds to a point on the infinitesimal homeostasis surface. The exact shape of the surface is determined by individual factors such as development, environmental exposures, psychological stress, drug effects, and aging.

The model of two-parameter homeostasis in Figure 2C does not incorporate progression from a healthy to a diseased condition. From our conceptual framework, when there is such progression, the value for the key dependent variable (in this case vesicular norepinephrine [NEv]) falls below the infinitesimal homeostasis surface.

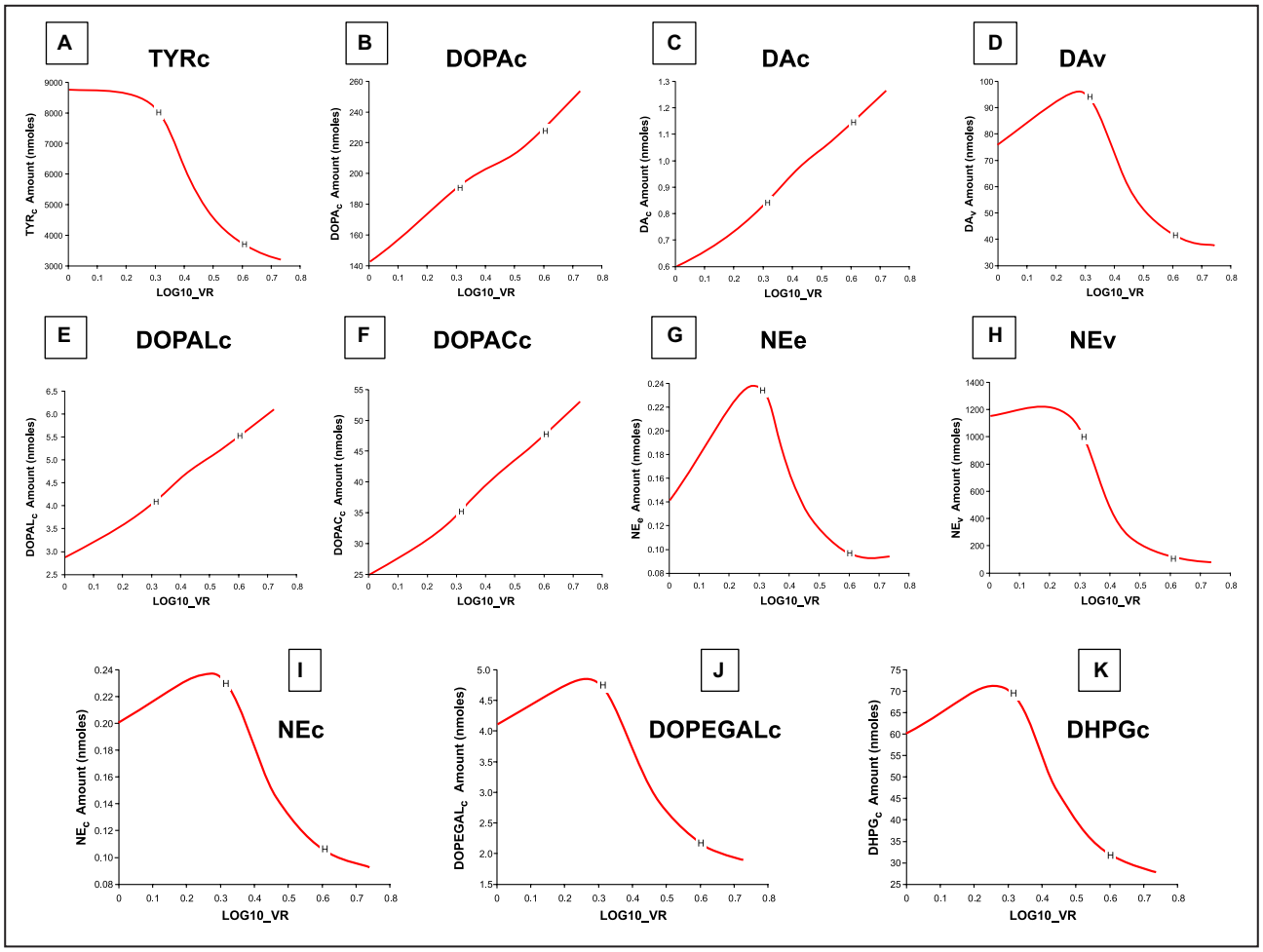

Figure 2. Model-predicted trends in amounts of reactants (nmoles).
The model predicts triphasic trends in cytoplasmic tyrosine, cytoplasmic norepinephrine, vesicular dopamine, vesicular norepinephrine, cytoplasmic norepinephrine, cytoplasmic 3,4-dihydroxyphenylglycolaldehyde, and cytoplasmic 3,4-dihydroxyphenylglycol and generally linear trends in cytoplasmic 3,4-dihydroxyphenylalanine, cytoplasmic dopamine, cytoplasmic 3,4-dihydroxyphenylacetaldehyde, and cytoplasmic 3,4-dihydroxyphenylacetic acid. H symbols correspond to Hopf bifurcations. DAc indicates cytoplasmic dopamine; DAv, vesicular dopamine; DHPGc, cytoplasmic 3,4-dihydroxyphenylglycol; DOPAc, cytoplasmic 3,4-dihydroxyphenylalanine; DOPACc, cytoplasmic 3,4-dihydroxyphenylacetic acid; DOPALc, cytoplasmic 3,4-dihydroxyphenylacetaldehyde; DOPEGALc, cytoplasmic 3,4-dihydroxyphenylglycolaldehyde; Log10_VR, log of vascular relaxation; NEc, cytoplasmic norepinephrine; NEe, extracellular fluid norepinephrine; NEv, vesicular norepinephrine; and TYRc, cytoplasmic tyrosine.

Effects of Cardiac Sympathetic Activation

The model examined the consequences of chronic cardiac sympathetic activation, either as a compensatory homeostatic response to systemic vasodilation or an anticipatory allostatic adjustment.[26] In principle, both would exert the same intra-neuronal effects; however, there are abundant empirical data about the effects of reflexive sympathetic stimulation.

Increased Rate Constant for NE Release

Administration of a drug that produces VR reflexively increases sympathetic noradrenergic outflows. By decreasing BP, VR releases sympathetic noradrenergic system outflows from baroreflexive restraint. Sympathetic noradrenergic system outflows to the heart and other organs increase. In the model, the reflexive increase in sympathetic noradrenergic system outflow increases the rate constant for NE release (kNE_Release) (Figure 1). This augments delivery of norepinephrine to the extracellular fluid and adrenoceptors, producing a vasoconstrictor effect that attenuates or eliminates the drug-evoked vasodilation. The reflexive increases in sympathetic noradrenergic system outflows to the heart and other organs maintain BP at or close to the baseline level.

Empirical data about effects of VR on BP were obtained from a study of infusion of nitroprusside on BP in the setting of trimethaphan-induced ganglion blockade.[27] Ganglion blockade eliminates baroreflexive

stimulation of sympathetic noradrenergic outflows. BP then falls approximately linearly as a function of the log of the nitroprusside infusion rate. In the model, the systolic BP is related to the log of vascular relaxation (Log10_VR).

With intact baroreflexes, when BP falls because of vascular relaxation sympathetic noradrenergic outflows increase reflexively. In humans, intravenous nitroprusside infusion increases cardiac sympathetic outflow as indicated by the rate of entry of norepinephrine into the cardiac venous drainage.[28] As a result of the reflexively increased sympathetic outflows, for a given rate of nitroprusside infusion the decrease in BP is attenuated.

One may presume that extracellular fluid norepinephrine (NEe) is directly related to kNE_Release if the pool of NEv is maintained. The concentration of norepinephrine at the neuroeffector junctions can be estimated from the plasma norepinephrine concentration during systemic norepinephrine infusion and during manipulations altering exocytotic norepinephrine release.[29]

Increased Rate Constant for TH

Sympathetic stimulation and exposure to stressors that increase sympathetic outflows do not normally decrease cardiac tissue norepinephrine concentrations. This is because of concurrently increased activity of TH, the rate-limiting enzyme in norepinephrine synthesis. Thus, when new synthesis of norepinephrine is prevented by alpha-methyl-para-tyrosine, which blocks TH, manipulations increasing cardiac sympathetic outflow decrease myocardial norepinephrine stores.[30] In the model, sympathetic stimulation increases the rate constant for TH (kTH), which maintains NEv despite increased kNE_Release.

Cardiac exocytotic norepinephrine release can increase by many-fold during severe stresses; however, TH activity increases by only at most 2- to 3-fold. In exercising healthy humans, cardiac norepinephrine spillover averages almost 18 times baseline, whereas in the same subjects cardiac DOPA spillover, an index of TH activity, averages 2.4 times baseline.[31]

Autotoxicity from Catecholaldehyde Buildup

Increased TH activity augments the production of dopamine in the neuronal cytoplasm, and this increases cytoplasmic DOPAL (DOPALc) production via oxidative deamination catalyzed by monoamine oxidase (increased kMAO_DA; Figure 1). Thus, mice that overexpress TH have increased striatal tissue DOPAL content.[32] Incubation of catecholaminergic rat pheochromocytoma PC12 cells with DOPA, the immediate precursor of dopamine, also increases endogenous DOPAL production.[33]

DOPAL inhibits TH[13] and LAAAD[14] and decreases synaptosomal dopamine uptake.[12] In the model DOPALc was presumed to exert equal inhibitory effects on kTH, the rate constant for LAAAD (kLAAAD), the rate constant vesicular uptake of cytoplasmic dopamine via the vesicular monoamine transporter (kVMAT_DA), and the rate constant for vesicular uptake of cytoplasmic norepinephrine mediated by the vesicular monoamine transporter (kVMAT_NE), while increasing the rate constants for vesicular leakage (kLeak) of dopamine (kLeak_DA) and of norepinephrine (kLeak_NE) (Figure S2).

Among the many proteins modified by DOPAL, one is αS. DOPAL potently oligomerizes αS,[14,34] and αS oligomers may be the toxic form of the protein, although this matter is unsettled. DOPAL-induced αS oligomers interfere with synaptic vesicular[7] and mitochondrial[16] functions. Vesicle permeabilization by αS oligomers[7] would increase values for kLeak in the model (Figure 1). Because of the absence of literature about the relative contributions of DOPAL, αS, and DOPAL-αS interactions to autotoxicity, the model lumps these 3 factors.

The model incorporates the catecholaldehyde 3,4-dihydroxyphenyglycolaldehyde (DOPEGAL), produced by the action of MAO on cytoplasmic norepinephrine (Figure 1); however, since there are no empirical data about DOPEGAL-induced toxicity or DOPEGAL-αS interactions in catecholaminergic neurons, the model does not include effects of DOPEGAL.

With reference to the homeostatic surface in Figure 2C, accumulation of DOPALc or of DOPALc-modified αS shrinks the homeostatic surface. When the homeostatic surface has shrunk sufficiently, the white disks “fall” from it.

To estimate the amount of DOPAL in the neuronal cytoplasm (DOPALc) we used empirical data about putamen tissue concentrations of DOPAL and 3,4-dihydroxyphenylacetic acid (DOPAC) (in nmol/g wet weight).[35,36] In control subjects, putamen DOPAL=0.316 nmol/g and DOPAC=2.687 nmol/g, so that the DOPAC/DOPAL concentration ratio=8.498. Assuming the same DOPAC/DOPAL ratio obtains in myocardial sympathetic nerves, for a cytoplasmic DOPAC amount of 25 nmoles, DOPALc=25/8.498=2.9 nmoles. Presuming ALDH is the sole route of metabolism of DOPAL, the DOPAC production rate=the DOPAL production rate=0.18 nmol/min.

In myocardium the rate of loss of 3,4-dihydroxyphenylglycol (DHPG) from the tissue is 1.2 nmol/min, which means the rate of metabolism of DOPEGAL to DHPG by aldehyde/aldose reductase is 1.2 nmol/min. Based on our unpublished observations from concurrent measurements of DOPEGAL and DHPG in sympathetic ganglion tissue from 3 control subjects, tissue DOPEGAL is about 7% of tissue DHPG.

The model includes progressive sympathetic noradrenergic denervation in LBDs, under the presumption that a loss of cardiac sympathetic nerves in LBDs is a result of a buildup of DOPAL. Our preliminary empirical data from patients with LBD indicate that by 16 years from symptom onset (a movement disorder or orthostatic intolerance due to orthostatic hypotension) there is about a 65% loss of cardiac sympathetic innervation; and published data from patients with PAF suggests a 41% decrease in innervation by 4.8 years.[37] In the model, neuronal loss is reflected by a decrease in the uptake of tyrosine—ie, decreased kTyr_Uptake.

Dopamine-beta-hydroxylase (DBH) is essential for intra-vesicular norepinephrine synthesis in sympathetic nerves; however, the rate-limiting enzyme in norepinephrine formation is TH.[38] Our model predictions agree with this, in that in controls kTH is 0.00020 min^{-1}, while rate constant for DBH (kDBH) is much higher at 0.018 min^{-1}. The rate of norepinephrine synthesis in sympathetic nerves depends not only on functional DBH enzyme but also on several other processes, which our model incorporates along with DBH. Mathematical application of the model has revealed that LBDs entail decreased catecholamine biosynthesis via TH and LAAAD, decreased vesicular uptake, and augmented vesicular leakage, all of which would be expected to decrease availability of substrate for DBH. The calculated kDBH is not decreased in patients with LBD.[5] Because of this, we did not include predictions about effects of alterations in kDBH.

Clinical Study Approval

Data were obtained from patients with LBDs and control subjects who had participated in ≥1 clinical research protocols approved by the Institutional Review Board of the National Institute of Neurological Disorders and Stroke. All research procedures were done after the participants had given written informed consent. Concerning the post-mortem observations, the National Institutes of Health Office of Human Subjects Research Protections determined that the post-mortem study was exempt from the requirement of Institutional Review Board approval. In all cases, the tissues were harvested for research purposes after the consent of the next of kin.

PET Scanning

The procedures for ^{18}F-DA PET scanning were the same as described previously.[5] For ^{18}F-DOPA PET scanning 7 mCi of ^{18}F-DOPA was administered without carbidopa pretreatment. PUT/OCC ratios and washout percents of ^{18}F-DOPA-derived radioactivity were calculated as also described previously.[18] Image analyses were done by personnel who were blinded as to the clinical diagnosis until the data were tabulated.

Follow-up PET scanning data were obtained from 2 groups, those with initially normal cardiac ^{18}F-DA-derived radioactivity and a subsequent decline (Group 1) and those with radioactivity that was already low upon initial testing (Group 2).

In a PD patient with normal myocardial ^{18}F-DA-derived radioactivity we tracked trends in radioactivity over more than 16 years of serial scanning. In another patient, PAF evolved over years to dementia with Lewy bodies and late PD. In this patient we reviewed data not only about cardiac ^{18}F-DA-derived radioactivity but also PUT/OCC ratio data from ^{18}F-DOPA scanning that were available for years before the onset of signs of central catecholamine deficiency.

Post-Mortem Data

Six patients with LBD who had undergone ^{18}F-DA PET scanning while alive underwent post-mortem tissue harvesting. Frozen apical myocardial tissue was assayed for contents of catecholamines, as described previously.[39]

Immunoreactive αS was assayed in the same myocardial specimens and in scalp skin when samples were available. Data about catecholamines and immunoreactive αS were also analyzed from post-mortem PD and control samples obtained under a Material Transfer Agreement with the Banner Sun Health Research Institute. The samples were embedded in optimum cutting temperature compound and sliced into 8- to 10-μm thick sections (Histoserv, Germantown, MD). αS was expressed relative to alpha-smooth muscle actin (SMA) in scalp skin or to cardiac troponin T (cTnT) in myocardium. The primary antibody to αS was mouse IgG1 monoclonal anti-αS (1:1000; Santa Cruz Biotechnology, Santa Cruz, CA), to SMA was mouse IgG2a monoclonal anti-SMA (1:400; Santa Cruz Biotechnology), and to cTnT was mouse IgG2a monoclonal human anti-cTnT (1:250; Pel-Freez Biologicals). The secondary antibodies for visualizing the immunoreactions were Alexa 488-conjugated anti-mouse IgG1, Alexa 555-conjugated anti-rabbit, and Alexa 647-conjugated anti-mouse IgG2a (Thermo Scientific, Inc, Rockford, IL). Immunofluorescence confocal microscopy was done using a Zeiss LSM 880 confocal laser scanning microscope (Carl Zeiss, Oberkochen, Germany).

RESULTS

Model-Predicted Changes in Levels of Reactants

Figure 2 shows model-predicted changes in levels of the 11 reactants as a function of Log10_VR. In general, levels of NEv, cytoplasmic tyrosine, vesicular dopamine, and

cytoplasmic DHPG decreased in a triphasic manner, while levels of cytoplasmic 3,4-dihydroxyphenylalanine, cytoplasmic dopamine, DOPALc, and cytoplasmic DOPAC increased approximately linearly.

Model-Predicted Triphasic Decline in NEv in LBDs

The model predicted a triphasic curvilinear relationship between NEv and Log10_VR (Figure 2H). At low values of Log10_VR, NEv was maintained and actually increased (Phase 1). At higher Log10_VR values NEv decreased markedly (Phase 2). Finally, NEv decreased slowly at high Log10_VR values (Phase 3). As shown in Figure 2, the 3 phases were separated by Hopf bifurcations (marked by H), indicating a segment involving oscillations of NEv.

Presuming a linear relationship between Log10_VR and time, with the onset of symptoms after 80% loss of NEv, Phase 2 would last about 4 years (Figure 3).

Individual data were analyzed from 3 patients with LBD with initially normal cardiac ^{18}F-DA-derived radioactivity (Group 1) and 9 with initially low radioactivity

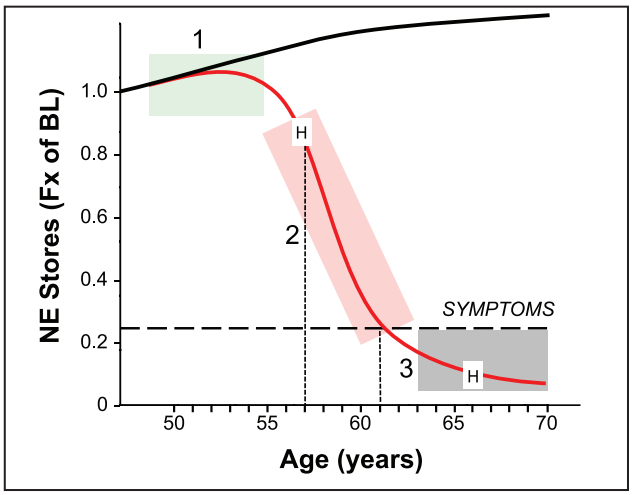

Figure 3. Model-predicted trends in myocardial norepinephrine stores as a function of age, with (red curve) and without (black curve) effects of cytoplasmic 3,4-dihydroxyphenylacetaldehyde on intra-neuronal reactions. Reactions affected by cytoplasmic 3,4-dihydroxyphenylacetaldehyde are depicted pictorially in Figure S2. When effects of cytoplasmic 3,4-dihydroxyphenylacetaldehyde are included (red curve), values for myocardial vesicular norepinephrine stores expressed as a fraction of the baseline value change in 3 phases (1 green, 2 pink, and 3 gray). Symptoms are presumed to occur when vesicular norepinephrine falls <25% of baseline (horizontal dashed line). A Hopf bifurcation (H) occurs at about the transition from Phase 1 to Phase 2. About 4 years intervene between Hopf bifurcation (H) and symptom onset (vertical dotted lines). When effects of cytoplasmic 3,4-dihydroxyphenylacetaldehyde are not included (black curve), vesicular norepinephrine increases over time, there is no Hopf bifurcation, and symptomatic disease does not develop. Fx of BL indicates fraction of the baseline value.

(Group 2) (Table S4). In the Group 1 subjects radioactivity declined exponentially at a rate of 7.8% per year. Among Group 2 subjects ^{18}F-DA-derived radioactivity during follow-up remained below the lower limit of normal.

Six patients with autopsy-proven LBDs had ^{18}F-DA PET scanning while alive and had post-mortem tissue harvesting. All 6 had markedly decreased apical myocardial concentrations of norepinephrine and dopamine (Table S5). The same patients had low interventricular septal myocardial concentrations of ^{18}F-DA-derived radioactivity.

In a patient with PD who was followed with serial ^{18}F-DA scanning over almost 17 years, during the first 8 years there was no clear trend in septal myocardial ^{18}F-DA-derived radioactivity (Figure 4). Then ^{18}F-DA-derived radioactivity fell rapidly, with about an 80% decline over the next 4.5 years. For the remainder of the follow-up period there was no further trend in radioactivity. The model-predicted triphasic curve applied well to the time-related changes in ^{18}F-DA-derived radioactivity in this patient (manually placed blue curve in Figure 3A).

A patient with PAF (Group 2, Patient 1 in Table S3) reported the onset of visual hallucinations at about 2 years of follow-up. At about 4 years the patient was diagnosed with dementia with Lewy bodies, and he developed parkinsonism late in the disease course. As shown in Figure 4B, during follow-up the patient's PUT/OCC ratio of ^{18}F-DOPA-derived radioactivity decreased rapidly; the relationship between the PUT/OCC ratio and years of follow-up was triphasic. The patient died, was autopsied, and was found to have brainstem Lewy bodies, markedly decreased myocardial catechol contents (Patient LBD2 in Table S4), and low PUT dopamine content (4.1 pmol/mg wet weight, about 30% of control).

Dependence of the Triphasic Decline on DOPALc

When the model did not include dependences of the rate constant for TYR uptake (kTYR_Uptake), kTH, kLAAAD, kVMAT_DA, kVMAT_NE, the rate constant for U1 (kU1), or kLeak on DOPALc, there was no model-predicted decline in NEv (Figure 3, black curve). NEv actually was predicted to increase slightly over years.

Model-Predicted Effects of Genetic Mutations

We queried the effects of congenitally decreased kTH, kLAAAD, the rate constant for MAO activing on cytoplasmic DA (kMAO_DA), kVMAT_DA, the rate constant for ALDH (kALDH), and kU1 on the relationship of NEv versus Log10_VR (Figure S3). Decreasing

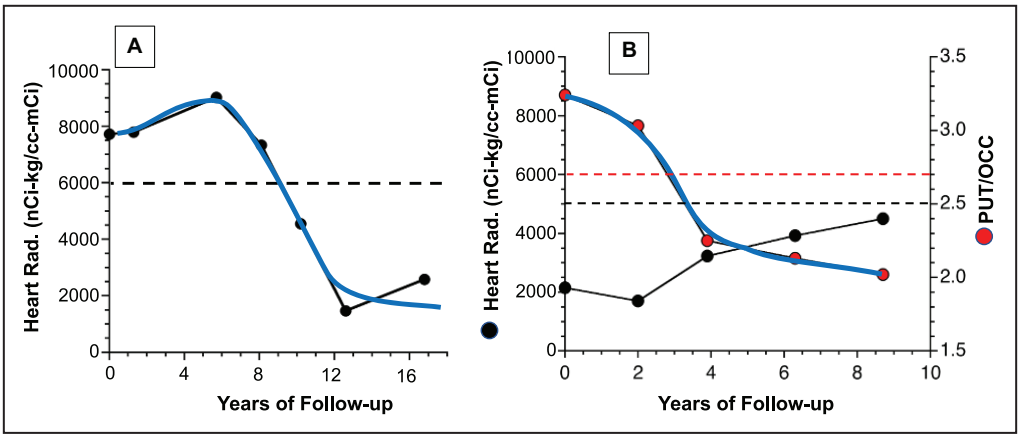

Figure 4. Empirical data for trends in indices of myocardial noradrenergic and putamen dopaminergic innervation during longitudinal follow-up of patients with Lewy body diseases. Blue curves of best fit placed manually. (**A**) Interventricular septal myocardial concentrations of 18F-dopamine-derived radioactivity (in units of nanoCuries (nCi)/cc adjusted for the radioactive dose in milliCuries (mCi) per kg of body mass) during longitudinal follow-up of a patient with Parkinson disease. (**B**) Myocardial 18F-dopamine-derived radioactivity concentrations (black circles) and concurrent putamen/occipital cortex ratios of 18F-3,4-dihydroxyyphenylalanine (^{18}F-DOPA)-derived radioactivity (red circles) during longitudinal follow-up of a patient with pure autonomic failure who developed dementia after about 4 years and parkinsonism after about 8 years. In the patient with Parkinson disease in (**A**), 18F-dopamine-derived radioactivity was above the lower limit of normal (horizontal black dashed line) for about 8 years and then rapidly decreased. In the patient with pure autonomic failure (PAF) in (**B**) 18F-dopamine-derived radioactivity was low at the time of initial evaluation and remained sub-normal. The putamen/occipital cortex ratio of 18F-3,4-dihydroxyphenylalanine-derived radioactivity was above the lower limit of normal (horizontal red dashed line) for about 3 years and then rapidly decreased. Note the triphasic declines in 18F-dopamine-derived radioactivity in the patient with Parkinson disease and of the putamen/occipital cortex ratio of ^{18}F-3,4-dihydroxyphenylalanine-derived radioactivity in the patient with PAF during longitudinal follow-up, as predicted by the model. PUT/OCC indicates putamen/occipital cortex.

kVMAT_DA or kALDH by 30% shifted the curve to the left (Figure S3A and S3B), indicating earlier depletion of vesicular norepinephrine stores. These shifts were associated with changes in the occurrence of Hopf bifurcations (H marks in the curves in Figure S3). The largest shifts were for 30% decreases in kTH (Figure S3E) and kMAO_DA (Figure S3F).

Model-Predicted Effects of Treatments

MAO inhibition decreasing the rate constant for MAO acting on cytoplasmic DA (kMAO_DA) and the rate constant for MAO acting on cytoplasmic NE (kMAO_NE) by 30% beginning at the first Hopf bifurcation rapidly increased NEv, with a subsequent decline (blue curve and arrow in Figure S4A). The same treatment but initiated after symptoms resulted in a smaller rapid increase in NEv and a brief asymptomatic period (green curve and arrow).

The addition of a treatment inhibiting the influences of DOPALc on the rate constants kTH, kLAAAD, kMAO_DA, kVMAT_DA, kALDH, and kU1 (ie, mimicking the effects of treatment with an antioxidant to mitigate DOPALc-αS interactions) exerted little effect, prolonging the asymptomatic period by about 1 year (Figure S4B, magenta curve).

Post-Mortem Immunoreactive αS in Skin and Myocardium and Myocardial Norepinephrine

According to the model, there should be an accumulation of αS in the myocardium in patients with LBD, associated with decreased NEv. One half of the 14 patients with LBD had elevated post-mortem immunoreactive αS adjusted for cTnT in the myocardium, while all 14 had elevated αS adjusted for SMA in arrector pili muscles in scalp skin (Figure 5A). Twelve of the 14 patients with LBD had both elevated arrector pili αS/SMA ratios and myocardial norepinephrine content below the control range (Figure 5B).

All the patients with LBDs had αS/cTnT ratios in myocardium that were above the control range also had αS/SMA ratios in arrector pili muscles that were above the control range (Figure 5A). Similarly, all patients with LBDs and low myocardial norepinephrine had elevated αS/SMA ratios (Figure 5B).

DISCUSSION

We report a computational model that predicts the progression of cardiac catecholamine deficiency in

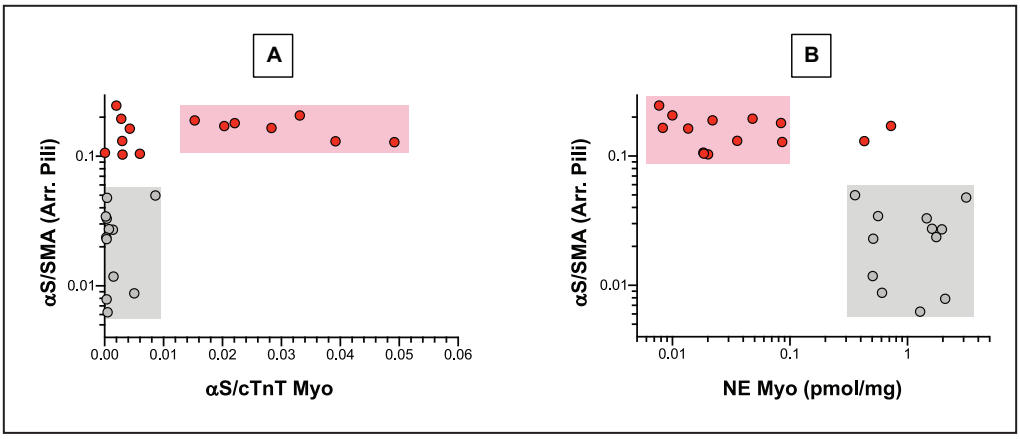

Figure 5. Post-mortem immunoreactive αS/smooth muscle actin in arrector pili muscles in scalp skin, expressed as functions of (**A**) apical myocardial αS/cardiac-specific troponin T (αS/cardiac troponin T) and (**B**) Apical myocardial norepinephrine content in patients with Lewy body diseases (red) and control subjects (gray). Light gray rectangles placed to indicate ranges of control values and pink rectangles values in Patients with Lewy body diseases who are outside the control ranges. Note that in **(A)** all patients with Lewy body diseases with elevated myocardial αS/cardiac troponin T ratios and in **(B)** all patients with Lewy body diseases with low apical myocardial norepinephrine levels have elevated arrector pili αS/smooth muscle actin ratios. αS indicates alpha-synuclein; Arr. Pili, arrector pili muscles; cTnT, cardiac troponin T; Myo, apical myocardial; and SMA, alpha smooth muscle actin.

LBDs. The model incorporates effects of homeostatic or allostatic increases in sympathetic noradrenergic outflow to the heart and autotoxicity from DOPAL. Key predictions from the model are (A) triphasic progression of catecholamine deficiency, (B) particular effects of genetic variants of intra-neuronal enzymes and processes on that progression, (C) effects of treatments that decrease DOPAL production or actions; and (D) cytoplasmic accumulation of αS in a manner associated with DOPAL buildup and catecholamine depletion. Empirical in vivo and post-mortem data largely confirm these predictions.

Catecholamine Deficiency in LBDs Progresses in 3 Phases

Longitudinal follow-up studies of patients with PD have suggested that the pattern of progression fits better with an inverse exponential curve than with a downsloping straight line.[9] These studies followed patients from the onset of symptomatic PD; however, according to our model, by the time a patient manifests symptomatically the loss of vesicular catecholamine stores is already advanced. The model predicts a critically important preclinical phase (Phase 1). Before the reported inverse exponential decline neurotransmitter stores are generally maintained. The reported inverse exponential curve represents rapid effects of dyshomeostasis in Phase 2 followed by a slower further decline during advanced disease in Phase 3.

To test the prediction that a triphasic pattern characterizes the loss of vesicular norepinephrine stores in cardiac sympathetic nerves we used empirical serial data about myocardial ^{18}F-DA-derived radioactivity, which is a validated in vivo biomarker of cardiac noradrenergic innervation.[17] One of our patients with PD underwent serial cardiac ^{18}F-DA PET scanning over almost 17 years (Figure 4A). As predicted by the model, ^{18}F-DA-derived radioactivity was normal upon initial evaluation and during 8 years of follow-up (Phase 1). Thereafter the radioactivity fell rapidly and substantially, with about an 80% decline over 4.5 years (Phase 2). Subsequently, ^{18}F-DA-derived radioactivity remained subnormal during further follow-up over several years (Phase 3). These data demonstrate the model-predicted triphasic curve for the decline in NEv.

The findings in 1 of our patients with PAF indicated the same triphasic temporal pattern of catecholamine loss can obtain in the nigrostriatal system of the brain (Figure 4B). The patient had PAF that progressed to dementia with Lewy bodies. As is typical of PAF, upon initial evaluation cardiac ^{18}F-DA-derived radioactivity was already low, and the PUT/OCC ratio of ^{18}F-DOPA-derived radioactivity was normal (Phase 1). During follow-up, the PUT/OCC ratio declined rapidly over a few years (Phase 2). Post-mortem analyses confirmed the co-occurrence of markedly decreased myocardial norepinephrine content, low putamen dopamine content, and brainstem LBs in this patient.

A triphasic disease progression pattern has been noted in other clinical conditions such as Alzheimer disease,[40] bicuspid aortic stenosis,[41] and post-myocarditis cardiomyopathy.[42] No previous model of LBDs has been applied to the preclinical period.

Increases in Cytosolic Dopamine and DOPAL as Part of the Pathogenetic Process

According to the model, decreased vesicular uptake coupled with increased TH activity results in a progressive increase in cytoplasmic dopamine levels. Empirical data support both decreased vesicular monoamine transporter activity[43] and increased cytoplasmic dopamine in PD.[44]

We did not detect DOPAL in any myocardial sample. An explanation may be extensive binding of DOPAL to intracellular peptides or proteins.[14] Consistent with this possibility, a recent study identified covalent adducts of DOPAL with L-cysteine and carnosine.[45]

The model does not include the potential of DOPEGAL as an autotoxic factor. Burke et al reported that exogenously administered DOPEGAL is toxic to rat pheochromocytoma PC12 cells,[46] and recent literature has provided evidence that exogenously administered DOPEGAL is toxic to myofibroblasts.[47] PubMed searches related to endogenous DOPEGAL yielded no study describing DOPEGAL levels in sympathetically innervated organs. This may be related to the challenge of accurately measuring this catecholaldehyde in body fluids and tissues.

Our model is a mechanistic model that generates testable predictions for the disease course based on empirical data about the disease processes and on theoretical understanding about how these processes are inter-related. We did not evaluate the model by calculations of true positives, false positives, etc., or train the model, since the purpose was not to establish diagnosis (for which these calculations would be appropriate) but to model the underlying physiological processes that impact disease progression. To refine the model, more empirical data are needed, especially about DOPAL-αS interactions in clinical samples.

Model-Predicted Effects of Genetic Variations on the Triphasic Decline

The model was tested by comparing predictions with empirical data for the effects of specific genetic variants on the onset of the triphasic decline in vesicular catecholamine stores (Figure S3). As discussed in detail below, all the model-predicted effects of genetic variations have empirical support from animal models.

Congenitally decreased ALDH activity produces a lifetime increase in DOPALc, and mice with double knockout of the genes encoding mitochondrial and cytosolic ALDH have aging-related central dopaminergic neurodegeneration and motor dysfunction.[48] The model predicted that genetically determined decreased VMAT2 activity would result in relatively early depletion of catecholamine stores (Figure 4B). In confirmation of this prediction, mice with congenital very low VMAT2 activity have decreased catecholamine contents in the brain and heart.[39,49]

Regarding predictions based on genetic variants in reactions in sympathetic nerves, there are reports about the extents of decrease in transporter or enzyme activities in affected patients with genetic deficiencies of VMAT2, MAO-A, or LAAAD. Genetic VMAT2 deficiency manifests as a lethal pediatric disease that includes parkinsonism. In affected members of a consanguineous family transmitting mutation of the *SLC18A2* gene encoding VAMT2, transporter activity was reported to be decreased by ≥90% based on incubation of membrane preparations with ^{3}H-serotonin.[50] MAO-A deficiency is transmitted as an X-linked trait; affected males have virtually no fibroblast MAO-A activity, while carriers have about 30% of normal activity.[51] In patients with genetic LAAAD deficiency, enzymatic activity can be undetectable.[52] In a screening neonatal study, 3-O-methyl DOPA in blood spots was increased by about 3-fold, suggesting about one third of normal enzyme activity.[53] We therefore used an estimated 30% decrease in enzyme or transporter activities, which we believe was reasonable based on the above literature.

Implications for Preclinical Biomarkers

The results emphasize the importance of identifying presymptomatic biomarkers to detect the transition from Phase 1 to Phase 2. As demonstrated by the longitudinal follow-up data in LBD cases followed over many years, trends in ^{18}F-DA-derived radioactivity may identify the key transition from Phase 1 to Phase 2. Data from the prospective NINDS PDRisk study (NIH Clinical Protocol 09N0010, "Biomarkers of Risk of Parkinson Disease") fit with this prediction,[54] by showing that low ^{18}F-DA-derived radioactivity in at-risk healthy individuals identified those who later developed symptomatic PD (Phase 2–3).

Another promising preclinical biomarker of LBDs is increased αS in sympathetic nerves in skin biopsies. Patients with Lewy body forms of neurogenic orthostatic hypotension have increased αS/smooth muscle actin (SMA) ratios in cutaneous arrector pili muscles, blood vessels, and sweat glands, in a manner related to low myocardial ^{18}F-DA-derived radioactivity.[55] In the current study, all the patients with LBDs who had low myocardial norepinephrine levels also had elevated αS/SMA ratios in arrector pili muscles from scalp skin (Figure 5). Longitudinal follow-up studies are needed to document whether analysis of αS/SMA ratios can detect the transition from Phase 1 to Phase 2.

Implications for Treatment

The present model predicts which interventions might be beneficial and, importantly, the optimal timing for the

interventions to be effective. For instance, the model predicts that MAO inhibition should immediately increase catecholamine stores (Figure S4A) and thereby improve symptoms temporarily. This prediction is confirmed by review of empirical data from the ADAGIO (Attenuation of Disease Progression With Azilect Given Once Daily) multi-center clinical trial of the MAO inhibitor rasagiline (Figure S4C).[19] The model predicts that the same intervention but begun at the transition from Phase 1 to Phase 2 would substantially delay the onset of symptoms (Figure S4A).

The model presumes that DOPALc inhibits several reactions in sympathetic noradrenergic nerves—TH, LAAAD, vesicular uptake, and neuronal reuptake—while increasing leakage from the vesicles to the cytoplasm. These effects cause the triphasic decline in NEv, since the triphasic progression pattern is not predicted when they are excluded (Figure 3). According to the model, however, in order to slow the decline of NEv by inhibiting DOPALc effects there would have to be very substantial attenuation of those effects. A 30% decrease from the start of Phase 2 would only slightly delay symptom onset (Figure S4B).

Limitations

Although DOPAL effects are sufficient and provide a parsimonious explanation, there is no evidence that DOPAL actually causes the progression of catecholamine deficiency in LBDs. The catecholaldehyde hypothesis remains a hypothesis. There are probably several other models that would predict a triphasic decline in norepinephrine stores, based on compensatory increases in nerve pathway traffic and toxicity from downstream intra-neuronal consequences of the increased traffic. To be acceptable, however, these would also have to predict empirical data about levels of the reactants and the effects of genetic predispositions and treatments.

Our model does not include several processes that likely would be required for a comprehensive picture over the lifespan, such as neurogenesis, neuroplasticity, or resilience.

The exact meaning of "interactions" of DOPAL with αS is ambiguous, because the relative roles of enzymatic or spontaneous catecholamine oxidation and αS in PD pathogenesis[56] have not been clarified.

The model-predicted triphasic decline in NEv is expressed as a function of cumulative effects of cardiac sympathetic activation, not time. We assumed a linear relationship between Log10_VR and follow-up years in LBDs. There are no empirical data to support this assumption.

Among the patients with LBDs, one half had myocardial αS/cTnT ratios within the control range. We used post-mortem myocardial αS/cTnT ratios to adjust αS signal intensities for the amounts of tissue in the samples. Since all the patients with LBDs had arrector pili αS/SMA ratios above the control range, the relationship between αS deposition in the skin and αS deposition in the myocardium seems to be complex. The implications for using cutaneous αS/SMA ratios in sympathetic noradrenergically innervated structures as in vivo biomarkers of myocardial αS deposition remain to be determined.

Perspective

We envision further development of mathematical modeling to enable predictions about complex interactions among genetic predispositions, environmental exposures, and drugs in the clinical manifestations and treatment of catecholaminergic neurodegeneration. More generally, computational modeling holds promise for enhancing patient-oriented research about autonomic and catecholamine-related disorders.

ARTICLE INFORMATION

Received October 21, 2021; accepted March 15, 2022.

Affiliations

Autonomic Medicine Section, Clinical Neurosciences Program, Division of Intramural Research, National Institute of Neurological Disorders and Stroke, National Institutes of Health, Bethesda, MD (D.S.G., P.S., R.I.); Mathematical Sciences, University of Alabama at Huntsville, Huntsville, AL (M.J.P.); and Tel Aviv University Sackler Faculty of Medicine and Chaim Sheba Medical Center, Tel HaShomerIsrael, (Y.S.).

Acknowledgments

We thank Carel Jonkhout for recent contributions to upgrading CI_MatContL. Author Contributions: David S. Goldstein: literature search, figures, study design, data collection, data analysis, data interpretation, writing; Mark Pekker: literature search, study design, data analysis, data interpretation, writing; Patti Sullivan: data collection, data analysis, reviewing and critique comments; Risa Isonaka: literature search, data collection, data analysis, reviewing and critique comments, writing; Yehonatan Sharabi: literature search, study design, data analysis, data interpretation, writing.

Sources of Funding

The research reported here was supported by the Division of Intramural Research, National Institutes of Health, NINDS.

Disclosures

None.

Supplemental Material

Tables S1–S5
Figures S1–S4
Reference 57

REFERENCES

1. Spillantini MG, Schmidt ML, Lee VM, Trojanowski JQ, Jakes R, Goedert M. Alpha-synuclein in Lewy bodies. *Nature*. 1997;388:839–840. doi: 10.1038/42166
2. Kish SJ, Shannak K, Hornykiewicz O. Uneven pattern of dopamine loss in the striatum of patients with idiopathic Parkinson's disease. Pathophysiologic and clinical implications. *N Engl J Med*. 1988;318:876–880. doi: 10.1056/NEJM198804073181402
3. Goldstein DS, Holmes C, Cannon RO 3rd, Eisenhofer G, Kopin IJ. Sympathetic cardioneuropathy in dysautonomias. *N Engl J Med*. 1997;336:696–702. doi: 10.1056/NEJM199703063361004

4. Goldstein DS, Sharabi Y. The heart of PD: Lewy body diseases as neurocardiologic disorders. *Brain Res*. 2019;1702:74–84. doi: 10.1016/j.brainres.2017.09.033
5. Goldstein DS, Pekker MJ, Eisenhofer G, Sharabi Y. Computational modeling reveals multiple abnormalities of myocardial noradrenergic function in Lewy body diseases. *JCI Insight*. 2019;5:e130441. doi: 10.1172/jci.insight.130441
6. Goldstein DS, Holmes C, Kopin IJ, Sharabi Y. Intra-neuronal vesicular uptake of catecholamines is decreased in patients with Lewy body diseases. *J Clin Invest*. 2011;121:3320–3330. doi: 10.1172/JCI45803
7. Plotegher N, Berti G, Ferrari E, Tessari I, Zanetti M, Lunelli L, Greggio E, Bisaglia M, Veronesi M, Girotto S, et al. DOPAL derived alpha-synuclein oligomers impair synaptic vesicles physiological function. *Sci Rep*. 2017;7:40699. doi: 10.1038/srep40699
8. Polinsky RJ, Goldstein DS, Brown RT, Keiser HR, Kopin IJ. Decreased sympathetic neuronal uptake in idiopathic orthostatic hypotension. *Ann Neurol*. 1985;18:48–53. doi: 10.1002/ana.410180109
9. Hilker R, Schweitzer K, Coburger S, Ghaemi M, Weisenbach S, Jacobs AH, Rudolf J, Herholz K, Heiss WD. Nonlinear progression of Parkinson disease as determined by serial positron emission tomographic imaging of striatal fluorodopa F 18 activity. *Arch Neurol*. 2005;62:378–382. doi: 10.1001/archneur.62.3.378
10. Goldstein DS. The catecholaldehyde hypothesis for the pathogenesis of catecholaminergic neurodegeneration: What we know and what we don't know. *Int J Mol Sci*. 2021;22:5999. doi: 10.3390/ijms22115999
11. Goldstein DS, Kopin IJ, Sharabi Y. Catecholamine autotoxicity. Implications for pharmacology and therapeutics of Parkinson disease and related disorders. *Pharmacol Ther*. 2014;144:268–282. doi: 10.1016/j.pharmthera.2014.06.006
12. Mattammal MB, Haring JH, Chung HD, Raghu G, Strong R. An endogenous dopaminergic neurotoxin: implication for Parkinson's disease. *Neurodegeneration*. 1995;4:271–281. doi: 10.1016/1055-8330(95)90016-0
13. Mexas LM, Florang VR, Doorn JA. Inhibition and covalent modification of tyrosine hydroxylase by 3,4-dihydroxyphenylacetaldehyde, a toxic dopamine metabolite. *Neurotoxicology*. 2011;32:471–477. doi: 10.1016/j.neuro.2011.03.013
14. Jinsmaa Y, Sharabi Y, Sullivan P, Isonaka R, Goldstein DS. 3,4-Dihydroxyphenylacetaldehyde-induced protein modifications and their mitigation by N-acetylcysteine. *J Pharmacol Exp Ther*. 2018;366:113–124. doi: 10.1124/jpet.118.248492
15. Mattammal MB, Chung HD, Strong R, Hsu FF. Confirmation of a dopamine metabolite in parkinsonian brain tissue by gas chromatography-mass spectrometry. *J Chromatogr*. 1993;614:205–212. doi: 10.1016/0378-4347(93)80310-Z
16. Sarafian TA, Yacoub A, Kunz A, Aranki B, Serobyan G, Cohn W, Whitelegge JP, Watson JB. Enhanced mitochondrial inhibition by 3,4-dihydroxyphenyl-acetaldehyde (DOPAL)-oligomerized alpha-synuclein. *J Neurosci Res*. 2019;97:1689–1705. doi: 10.1002/jnr.24513
17. Lamotte G, Holmes C, Wu T, Goldstein DS. Long-term trends in myocardial sympathetic innervation and function in synucleinopathies. *Parkinsonism Relat Disord*. 2019;67:27–33. doi: 10.1016/j.parkreldis.2019.09.014
18. Goldstein DS, Holmes C, Bentho O, Sato T, Moak J, Sharabi Y, Imrich R, Conant S, Eldadah BA. Biomarkers to detect central dopamine deficiency and distinguish Parkinson disease from multiple system atrophy. *Parkinsonism Relat Disord*. 2008;14:600–607. doi: 10.1016/j.parkreldis.2008.01.010
19. Olanow CW, Rascol O, Hauser R, Feigin PD, Jankovic J, Lang A, Langston W, Melamed E, Poewe W, Stocchi F, et al. A double-blind, delayed-start trial of rasagiline in Parkinson's disease. *N Engl J Med*. 2009;361:1268–1278. doi: 10.1056/NEJMoa0809335
20. Rascol O, Hauser RA, Stocchi F, Fitzer-Attas CJ, Sidi Y, Abler V, Olanow CW, Investigators AFU. Long-term effects of rasagiline and the natural history of treated Parkinson's disease. *Mov Disord*. 2016;31:1489–1496. doi: 10.1002/mds.26724
21. Bindel D, Friedman M, Govaerts W, Hughes J, Kuznetsov YA. Numerical computation of bifurcations in large equilibrium systems in matlab. *J Comput Appl Math*. 2014;261:232–248. doi: 10.1016/j.cam.2013.10.034
22. Bindel D, Govaerts W, Hughes J, Kuznetsov YA, Pekker M, Veldman D. CL_MATCONTL2015p0: continuation toolbox in MATLAB. 2015. http://uahedu/faculty/pekker
23. Demmel JW, Dieci L, Friedman MJ. Computing connecting orbits via an improved algorithm for continuing invariant subspaces. *SIAM J Sci Comput*. 2000;22:81–94. doi: 10.1137/S1064827598344868
24. Golubitsky M, Stewart I, Antoneli F, Huang Z, Wang Y. Input-output networks, singularity theory, and homeostasis. *Adv Dyn Optim Comput*. 2020;304. doi: 10.1007/978-3-030-51264-4_2
25. Nijhout HF, Best J, Reed MC. Escape from homeostasis. *Math Biosci*. 2014;257:104–110. doi: 10.1016/j.mbs.2014.08.015
26. Sterling P. *What is Health? Allostasis and the Evolution of Human Design*. MIT Press; 2020.
27. D'Oyley HM, Tabrizchi R, Pang CC. Effects of vasodilator drugs on venous tone in conscious rats. *Eur J Pharmacol*. 1989;162:337–344. doi: 10.1016/0014-2999(89)90297-5
28. Ros M, Azevedo ER, Newton GE, Parker JD. Effects of nitroprusside on cardiac norepinephrine spillover and isovolumic left ventricular relaxation in the normal and failing human left ventricle. *Can J Cardiol*. 2002;18:1211–1216.
29. Goldstein DS, Zimlichman R, Stull R, Keiser HR, Kopin IJ. Estimation of intrasynaptic norepinephrine concentrations in humans. *Hypertension*. 1986;8:471–475. doi: 10.1161/01.HYP.8.6.471
30. Bhagat B. The influence of sympathetic nervous activity on cardiac catecholamine levels. *J Pharmacol Exp Ther*. 1967;157:74–80.
31. Eisenhofer G, Rundqvist B, Friberg P. Determinants of cardiac tyrosine hydroxylase activity during exercise-induced sympathetic activation in humans. *Am J Physiol*. 1998;274:R626–R634. doi: 10.1152/ajpregu.1998.274.3.R626
32. Vecchio LM, Sullivan P, Dunn AR, Bermejo MK, Fu R, Masoud ST, Gregersen E, Urs NM, Nazari R, Jensen PH, et al. Enhanced tyrosine hydroxylase activity induces oxidative stress, causes accumulation of autotoxic catecholamine metabolites, and augments amphetamine effects in vivo. *J Neurochem*. 2021;158:960–979. doi: 10.1111/jnc.15432
33. Goldstein DS, Sullivan P, Cooney A, Jinsmaa Y, Sullivan R, Gross DJ, Holmes C, Kopin IJ, Sharabi Y. Vesicular uptake blockade generates the toxic dopamine metabolite 3,4-dihydroxyphenylacetaldehyde in PC12 cells: relevance to the pathogenesis of Parkinson's disease. *J Neurochem*. 2012;123:932–943. doi: 10.1111/j.1471-4159.2012.07924.x
34. Burke WJ, Kumar VB, Pandey N, Panneton WM, Gan Q, Franko MW, O'Dell M, Li SW, Pan Y, Chung HD, et al. Aggregation of alpha-synuclein by DOPAL, the monoamine oxidase metabolite of dopamine. *Acta Neuropathol*. 2008;115:193–203. doi: 10.1007/s00401-007-0303-9
35. Goldstein DS, Sullivan P, Holmes C, Kopin IJ, Basile MJ, Mash DC. Catechols in post-mortem brain of patients with Parkinson disease. *Eur J Neurol*. 2011;18:703–710. doi: 10.1111/j.1468-1331.2010.03246.x
36. Goldstein DS, Sullivan P, Holmes C, Miller GW, Alter S, Strong R, Mash DC, Kopin IJ, Sharabi Y. Determinants of buildup of the toxic dopamine metabolite DOPAL in Parkinson's disease. *J Neurochem*. 2013;126:591–603. doi: 10.1111/jnc.12345
37. Goldstein DS, Isonaka R, Holmes C, Ding YS, Sharabi Y. Cardiac sympathetic innervation and vesicular storage in pure autonomic failure. *Ann Clin Transl Neurol*. 2020;7:1908–1918. doi: 10.1002/acn3.51184
38. Nagatsu T, Levitt M, Udenfriend S. Tyrosine hydroxylase. The initial step in norepinephrine biosynthesis. *J Biol Chem*. 1964;239:2910–2917. doi: 10.1016/S0021-9258(18)93832-9
39. Goldstein DS, Sullivan P, Holmes C, Miller GW, Sharabi Y, Kopin IJ. A vesicular sequestration to oxidative deamination shift in myocardial sympathetic nerves in Parkinson disease. *J Neurochem*. 2014;131:219–228. doi: 10.1111/jnc.12766
40. Raket LL. Statistical disease progression modeling in Alzheimer disease. *Front Big Data*. 2020;3:24. doi: 10.3389/fdata.2020.00024
41. Kim D, Chae D, Shim CY, Cho IJ, Hong GR, Park K, Ha JW. Predicting disease progression in patients with bicuspid aortic stenosis using mathematical modeling. *J Clin Med*. 2019;8. doi: 10.3390/jcm8091302
42. Mason JW. Myocarditis and dilated cardiomyopathy: an inflammatory link. *Cardiovasc Res*. 2003;60:5–10. doi: 10.1016/S0008-6363(03)00437-1
43. Pifl C, Rajput A, Reither H, Blesa J, Cavada C, Obeso JA, Rajput AH, Hornykiewicz O. Is Parkinson's disease a vesicular dopamine storage disorder? Evidence from a study in isolated synaptic vesicles of human and nonhuman primate striatum. *J Neurosci*. 2014;34:8210–8218. doi: 10.1523/JNEUROSCI.5456-13.2014
44. Sackner-Bernstein J. Estimates of intracellular dopamine in Parkinson's disease: a systematic review and meta-analysis. *J Parkinsons Dis*. 2021;11:1011–1018. doi: 10.3233/JPD-212715
45. Crawford RA, Gilardoni E, Monroe TB, Regazzoni L, Anderson EJ, Doorn JA. Characterization of catecholaldehyde adducts with carnosine and l-cysteine reveals their potential as biomarkers of catecholaminergic stress. *Chem Res Toxicol*. 2021;34:2184–2193. doi: 10.1021/acs.chemrestox.1c00153

46. Burke WJ, Schmitt CA, Miller C, Li SW. Norepinephrine transmitter metabolite induces apoptosis in differentiated rat pheochromocytoma cells. *Brain Res*. 1997;760:290–293. doi: 10.1016/S0006-8993(97)00447-2
47. Monroe TB, Anderson EJ. A catecholaldehyde metabolite of norepinephrine induces myofibroblast activation and toxicity via the receptor for advanced glycation endproducts: mitigating role of l-carnosine. *Chem Res Toxicol*. 2021;34:2194–2201. doi:10.1021/acs.chemrestox.1c00262
48. Wey M, Fernandez E, Martinez PA, Sullivan P, Goldstein DS, Strong R. Neurodegeneration and motor dysfunction in mice lacking cytosolic and mitochondrial aldehyde dehydrogenases: implications for Parkinson's disease. *PLoS One*. 2012;7:e31522. doi: 10.1371/journal.pone.0031522
49. Taylor TN, Caudle WM, Shepherd KR, Noorian A, Jackson CR, Iuvone PM, Weinshenker D, Greene JG, Miller GW. Nonmotor symptoms of Parkinson's disease revealed in an animal model with reduced monoamine storage capacity. *J Neurosci*. 2009;29:8103–8113. doi: 10.1523/JNEUROSCI.1495-09.2009
50. Rilstone JJ, Alkhater RA, Minassian BA. Brain dopamine-serotonin vesicular transport disease and its treatment. *N Engl J Med*. 2013;368:543–550. doi: 10.1056/NEJMoa1207281
51. Peters TMA, Lammerts van Bueren I, Geurtz B, Coene KLM, de Leeuw N, Brunner HG, Jonsson JJ, Willemsen M, Wevers RA, Verbeek MM. Monoamine oxidase A activity in fibroblasts as a functional confirmation of MAOA variants. *JIMD Rep*. 2021;58:114–121. doi: 10.1002/jmd2.12194
52. Hyland K, Reott M. Prevalence of aromatic l-amino acid decarboxylase deficiency in at-risk populations. *Pediatr Neurol*. 2020;106:38–42. doi: 10.1016/j.pediatrneurol.2019.11.022
53. Burlina A, Giuliani A, Polo G, Gueraldi D, Gragnaniello V, Cazzorla C, Opladen T, Hoffmann G, Blau N, Burlina AP. Detection of 3-O-methyldopa in dried blood spots for neonatal diagnosis of aromatic L-amino-acid decarboxylase deficiency: the northeastern Italian experience. *Mol Genet Metab*. 2021;133:56–62. doi: 10.1016/j.ymgme.2021.03.009
54. Goldstein DS, Holmes C, Lopez GJ, Wu T, Sharabi Y. Cardiac sympathetic denervation predicts PD in at-risk individuals. *Parkinsonism Relat Disord*. 2018;52:90–93. doi: 10.1016/j.parkreldis.2017.10.003
55. Isonaka R, Rosenberg AZ, Sullivan P, Corrales A, Holmes C, Sharabi Y, Goldstein DS. Alpha-Synuclein deposition within sympathetic noradrenergic neurons is associated with myocardial noradrenergic deficiency in neurogenic orthostatic hypotension. *Hypertension*. 2019;73:910–918. doi: 10.1161/HYPERTENSIONAHA.118.12642
56. Roy S. Synuclein and dopamine: the Bonnie and Clyde of Parkinson's disease. *Nat Neurosci*. 2017;20:1514–1515. doi: 10.1038/nn.4660
57. Morrison PR. Temperature regulation in three central American mammals. *J Cell Comp Physiol*. 1946;27:125–137. doi: 10.1002/jcp.1030270302

SUPPLEMENTAL MATERIAL

Table S1. Initial reactant amounts, reaction rates, and rate constants in the kinetic model.

AMOUNTS

REACTANT		PARAMETER	VALUE	RANGE
1	TYRc	TYRc Amount	8747	
2	DOPAc	DOPAc Amount	142	105-200
3	DAc	DAc Amount	0.6	
4	DOPACc	DOPACc Amount	25	10-75
5	DAv	DAv Amount	76	30-110
6	NEv	NEv Amount	1150	885-1771
7	NEe	NEe Amount	0.14	
8	NEc	NEc Amount	2.1	
9	DHPGc	DHPGc Amount	60	47-165
10	DOPALc	DOPALc Amount	2.9	
11	DOPEGALc	DOPEGALc Amount	4.1	

RATES

REACTION		PARAMETER	VALUE	RANGE
1	TYR_Uptake	TYR Uptake Rate to TYRc	56	34-89
2	TYR_Loss	TYRc Loss Rate to ECF	54	33-87
3	TH	TYRc Conversion Rate to DOPAc	1.8	1.1-2.8
4	LAAAD	DOPAc Conversion Rate to DAc	1.5	1.2-1.8
5	DOPAc_Loss	DOPAc Exit Rate from the Model	0.22	0.15-0.33
6	Leak_DA	DAv Loss Rate to Cytoplasm	0.87	0.66-1.08
7	VMAT_DA	DAc Vesicular Uptake Rate	2.2	1.8-2.7
8	MAO_DA	DAc Conversion Rate to DOPACc	0.18	0.11-0.29
9	ALDH_DOPALc	DOPALc Conversion Rate to DOPACc	0.18	
10	DOPACc_Loss	DOPACc Exit Rate from the Model	0.18	0.11-0.29

11	DBH	DAv Conversion Rate to NEv	1.4	1.4-3.6
12	VMAT_NE	Vesicular Uptake Rate of NEc	14	11-22
13	Leak_NE	NEv Loss Rate to Cytoplasm	13	10-20
14	NE_Release	NEv Release Rate to ECF	2.6	1.4-3.7
15	U1	NEe Reuptake Rate to NEc	2.4	1.3-3.5
16	NEe_Loss	NEe Exit Rate from the Model	0.21	0.11-0.29
17	MAO_NE	NEc Conversion Rate to DHPGc	1.2	0.8-1.8
18	AR_DOPEGALc	DOPEGALc Conversion Rate to DHPGc	1.2	
19	DHPGc_Loss	DHPGc Exit Rate from the Model	1.2	0.8-1.8

Rate constants for 19 reactions were generated mathematically and are tabulated below.

RATE CONSTANTS

REACTION		**PARAMETER**	**VALUE**
1	kTYR_Uptake	TYR Uptake Rate to TYRc	56
2	kTYR_Loss	TYRc Loss Rate to ECF	54
3	kTH	TYRc Conversion Rate to DOPAc	0.00020
4	kLAAAD	DOPAc Conversion Rate to DAc	0.011
5	kDOPAc_Loss	DOPAc Exit Rate from the Model	0.0016
6	kLeak_DA	DAv Loss Rate to Cytoplasm	0.011
7	kVMAT_DA	DAc Vesicular Uptake Rate	3.76
8	kMAO_DA	DAc Conversion Rate to DOPACc	0.30
9	kALDH_DOPALc	DOPALc Conversion Rate to DOPACc	0.061
10	kDOPACc_Loss	DOPACc Exit Rate from the Model	0.0072
11	kDBH	DAv Conversion Rate to NEv	0.018
12	kVMAT_NE	Vesicular Uptake Rate of NEc	6.72
13	kLeak_NE	NEv Loss Rate to Cytoplasm	0.011
14	kNE_Release	NEv Release Rate to ECF	0.0023
15	kU1	NEe Reuptake Rate to NEc	17.1

16	kNEe_Loss	NEe Exit Rate from the Model	1.49
17	kMAO_NE	NEc Conversion Rate to DHPGc	0.57
18	kAR_DOPEGALc	DOPEGALc Conversion Rate to DHPGc	0.29
19	kDHPGc_Loss	DHPGc Exit Rate from the Model	0.020

All reactant amounts are in nmoles and all rates in nmoles/min. Listed ranges are based on 25% and 75% quartiles of empirical median values.[5] See Figure 1 for a pictorial representation of the reactants and reactions in the model.

Table S2. Model Equations.

In the equations below, several rate constants are listed that are nonlinear functions obtained from the curves approximating/interpolating the data. The Appendix contains the MATLAB code. The reactions are depicted pictorially in Figure 1.

The repressors are: kTH, a function of BP and kTH, kLAAAD, kVMAT_DA, kVMAT_NE, kU1, kTYR_Uptake, functions of DOPALc.

The activators are: kLeak_DA, kLeak_NE, functions of DOPALc.

(1) d[TYRc]/dt = kTYR_Uptake – (kTH + kTYR_Loss) * [TYRc]

(2) d[DOPAc]/dt = kTH * [TYRc] – (kDOPA_Loss + kLAAAD) * [DOPAc]

(3) d[DAc]/dt = kLAAAD * [DOPAc] + kLeak_DA * [DAv]
– (kMAO_DA + kVMAT_DA) * [DAc]

(4) d[DOPACc]/dt = kALDH_DOPALc*DOPALc – kDOPAC_Loss * [DOPACc]

(5) d[DAv]/dt = kVMAT_DA * [DAc] – (kLeak_DA + kDBH) * [DAv]

(6) d[NEv]/dt = kDBH * [DAv] + kVMAT_NE * [NEc]
– (kLeak_NE + kNE_Release) * [NEv]

(7) d[NEe]/dt = kNE_Release * [NEv] – kU1 * [NEe] - kNEe_Loss*NEe

(8) d[NEc]/dt = kLeak_NE*NEv + kU1*NEe - (kVMAT_NE + kMAO_NE) * [NEc];

(9) d[DHPGc]/dt = kAR_DOPEGALc*[DOPEGALc] – kDHPG_Loss * [DHPGc]

(10) d[DOPALc]/dt = kMAO_DA*[DAc] - kALDH_DOPALc*[DOPALc]

(11) d[DOPEGALc]/dt =kMAO_NE*[NEc] - kAR_DOPEGALc*[DOPEGALc]

where the reactant abbreviations were: (1) TYRc=cytoplasmic tyrosine, (2) DOPAc=cytoplasmic 3,4-dihydroxyphenylalanine, (3) DAv=vesicular dopamine, (4) DAc=cytoplasmic dopamine, (5) DOPACc=cytoplasmic 3,4-dihydroxyphenylacetic acid; (6) NEv=vesicular norepinephrine, (7) NEc=cytoplasmic norepinephrine, (8) DHPGc=cytoplasmic 3,4-dihydroxyphenylglycol; (9) NEe=norepinephrine in the extracellular fluid; (10) DOPALc=cytoplasmic 3,4-dihydroxyphenylacetaldehyde; (11) DOPEGALc=cytoplasmic 3,4-dihydroxyphenylglycolaldehyde.

Abbreviations: (1) TYR_Uptake=neuronal uptake of tyrosine, (2) TYR_Loss=loss of tyrosine from the nerves, (3) TH=tyrosine hydroxylase, (4) LAAAD=L-aromatic-amino-acid decarboxylase, (5) DOPA_Loss=loss of DOPAC from the nerves, (6) VMAT_DA=vesicular uptake of cytoplasmic DA via the VMAT, (7) MAO_DA=MAO acting on cytoplasmic DA, (8) DOPAC_Loss=loss of DOPAC from the nerves, (9) DBH=DA-beta-hydroxylase acting on vesicular DA to form vesicular NE, (10) Leak_DA=leakage of vesicular DA into the cytoplasm, (11) VMAT_NE=vesicular uptake of cytoplasmic NE via the VMAT, (12) MAO_NE=monoamine oxidase acting on cytoplasmic norepinephrine to form DHPG, (13) Leak_NE=leakage of vesicular NE into the cytoplasm, (14) NE_Release=NE release by vesicular exocytosis, (15) U1=neuronal uptake of NE via the cell membrane norepinephrine transporter (NET), (16) DHPG_Loss=loss of DHPG from the nerves, and (17) NE_Loss=loss of extracellular NE from the nerves.

Table S5. MATLAB function Parkinson_11d1.

For our ODE system, where the reactions and reactants are depicted in Figure 1, we have the following MATLAB function and subfunctions.

```
function out = Parkinson_11d1_symbolic()
out[1] = @init;
out[2] = @fun_eval;
end
% ------------------------------------------------------------------------
function x0 = init(logV)
%   TYRc DOPAc DAc DOPACc DAv NEv NEe NEc DHPGc DOPALc DOPEGALc
x0 = [8747 142  0.6 25   76  1150 0.14 20  60   2.9   4.1 ]';
end
% ------------------------------------------------------------------------
function dydt = fun_eval(~,y, logVR)
% unused parameter is t
% input: initial approximate rates r0 and initial reactants y0
% output: initial accurate rates r_s (scaled)
TYRc = y(1); DOPAc = y(2); DAc = y(3); DOPACc = y(4); DAv = y(5); NEv = y(6);
NEe = y(7); NEc = y(8); DHPGc = y(9); DOPALc = y(10); DOPEGALc = y(11);
%
kTYR_Uptake0  = 5.589189955455429e+01; %
kTYR_Loss   = 6.185036797562349e-03; %
kTH0     = 2.047996668888087e-04; % baseline, initial for DOPALc,
kLAAAD0    = 1.106515697265155e-02; % baseline, initial for DOPALc
kDOPAc_Loss  = 1.550214057463951e-03; %
kLeak_DA0   = 1.133781834294390e-02; % baseline, min, initial for DOPALc
kVMAT_DA0  = 3.755398997515088e+00; % baseline, initial for DOPALc
```

```
kMAO_DA   = 2.994784761187236e-01; %
kALDH_DOPALc = 6.196106402455661e-02; %
kDOPACc_Loss = 7.187483426848048e-03; %
kDBH     = 1.831006847954365e-02; %
kVMAT_NE0   = 7.056699257453658e-01;% baseline, initial for DOPALc
kLeak_NE0   = 1.121932409485655e-02;% baseline, min, initial for DOPALc
kNE_Release0 = 2.263253052406611e-03;% 14 baseline, kNE_Release varies
kU10     = 1.710237097742159e+01;% baseline, initial for DOPALc
kNEe_Loss  = 1.488636238775596e+00;%
kMAO_NE   = 5.915780655083667e-02;% , orig: 5.634076814365396e-01
kAR_DOPEGALc = 2.885746661016436e-01;%
kDHPGc_Loss = 1.971926885027911e-02;%
% repressor BP -> kTH, kNE_Release
  k1 = 83; % feedback parameters start here
  BP = 120 - k1*logVR; %
% ------------------------------------------------------------------------
x_BP = BP;
  x_BP_min = 50; % initial value of x_BP
  x_BP_max = 120;
% ------------------------------------------------------------------------
  y_kTH_BP_min = kTH0;
  y_kTH_BP_max = kTH0*2.5;
  n_kTH_BP = log(y_kTH_BP_min/y_kTH_BP_max)/(x_BP_min - x_BP_max);
kTH_BP = y_kTH_BP_max*exp(n_kTH_BP*(x_BP_min - x_BP));
% ------------------------------------------------------------------------
  y_kNE_Release_min = kNE_Release0;
  y_kNE_Release_max = kNE_Release0*4; % 0.0091;
```

```
  n_kNE_Release = log(y_kNE_Release_min/y_kNE_Release_max)/(x_BP_min - x_BP_max);
% 0.019804
kNE_Release = y_kNE_Release_max*exp(n_kNE_Release*(x_BP_min - x_BP));
% ------------------------------------------------------------------------
% repressor DOPALc: kTH, kLAAAD, kVMAT_DA, kVMAT_NE, kU1, kTYR_Uptake
x_DOP = DOPALc;
  x_DOP_min = 2.9;  % initial value of x_DOP
  K = 1.8; %
  n = 5;
  coef = 0.35;
% ------------------------------------------------------------------------
kTH_ = kTH0*((1 - coef)*K^n/(K^n + (x_DOP-x_DOP_min)^n) + coef);
kTH = kTH_BP + kTH_DOPALc - kTH0; % Step 3a,b
% ------------------------------------------------------------------------
kLAAAD = kLAAAD0*((1 - coef)*K^n/(K^n + (x_DOP-x_DOP_min)^n) + coef);
% ------------------------------------------------------------------------
kVMAT_DA = kVMAT_DA0*((1 - coef)*K^n/(K^n + (x_DOP-x_DOP_min)^n) + coef);
% ------------------------------------------------------------------------
kVMAT_NE = kVMAT_NE0*((1 - coef)*K^n/(K^n + (x_DOP-x_DOP_min)^n) + coef); %
% ------------------------------------------------------------------------
kU1 = kU10*((1 - coef)*K^n/(K^n + (x_DOP-x_DOP_min)^n) + coef);
% ------------------------------------------------------------------------
kTYR_Uptake = kTYR_Uptake0*((1 - coef)*K^n/(K^n + (x_DOP-x_DOP_min)^n) + coef);
% ------------------------------------------------------------------------
% activator DOPALc: kLeak_DA kLeak_NE,
  n_a = 4;
  K_a = 2.2;
```

```
  coef_a = 3;
kLeak_DA = kLeak_DA0*( (coef_a - 1)*(x_DOP - x_DOP_min)^n_a...
  /(K_a^n_a + (x_DOP - x_DOP_min)^n_a) + 1 );% Step 3d
% ------------------------------------------------------------------------
kLeak_NE = kLeak_NE0*( (coef_a - 1)*(x_DOP - x_DOP_min)^n_a...
  /(K_a^n_a + (x_DOP - x_DOP_min)^n_a) + 1 );% Step 3d
f1 = kTYR_Uptake - (kTYR_Loss+kTH)*TYRc; % 1, TYRc
f2 = kTH*TYRc - (kLAAAD+kDOPAc_Loss)*DOPAc; % 2, DOPAc
f3 = kLAAAD*DOPAc + kLeak_DA*DAv-(kVMAT_DA+kMAO_DA)*DAc; % 3, DAc
f4 = kALDH_DOPALc*DOPALc - kDOPACc_Loss*DOPACc; % 4, DOPACc rev
f5 = kVMAT_DA*DAc - (kLeak_DA+kDBH)*DAv; % 5, DAv
f6 = kDBH*DAv + kVMAT_NE*NEc - (kLeak_NE+kNE_Release)*NEv;% 6, NEv
f7 = kNE_Release*NEv - kU1*NEe - kNEe_Loss*NEe; % 7, NEe
f8 = kLeak_NE*NEv + kU1*NEe - (kVMAT_NE+kMAO_NE)*NEc; % 8, NEc
f9 = kAR_DOPEGALc*DOPEGALc - kDHPGc_Loss*DHPGc; % 9, DHPGc rev
f10 = kMAO_DA*DAc - kALDH_DOPALc*DOPALc; %10, DOPALc new
f11 = kMAO_NE*NEc - kAR_DOPEGALc*DOPEGALc; %11, DOPEGALc new
dydt = [f1; f2; f3; f4; f5; f6; f7; f8; f9; f10; f11];
end
```

Table S4, Individual data for interventricular septal myocardial ^{18}F-dopamine- (^{18}F-DA) derived radioactivity as a function of years of follow-up (F/u).

GROUP 1	N	Sex	Age	Diagnosis	Initial	F/u 1	F/u 2	F/u 3	F/u 4	F/u 5	F/u 6
F/u years	1	M	53	PD	0.0	1.3	5.7	8.1	10.2	12.6	16.8
^{18}F-DA	1				7723	7791	9027	7335	4547	1469	2582
^{18}F-DA Fx Initial	1				1.00	1.01	1.17	0.95	0.59	0.19	0.33
F/u years	2	M	53	PAF	0.0	1.8	3.8	7.7	10.1		
^{18}F-DA	2				7487	5654	3643	3192	3110		
^{18}F-DA Fx Initial	2				1.00	0.76	0.49	0.43	0.42		
F/u years	3	M	63	PD	0.0	2.9	4.0	6.4	13.4	16.8	
^{18}F-DA	3				6993	6110	8349	5190	6443	4061	
^{18}F-DA Fx Initial	3				1.00	0.87	1.19	0.74	0.92	0.58	
Mean F/u years					**0.0**	**1.9**	**4.1**	**6.7**	**11.3**	**14.7**	**16.8**
Mean ^{18}F-DA					**7401**	**6518**	**7006**	**5239**	**4700**	**2765**	**2582**
Mean ^{18}F-DA Fx					**0.75**	**0.66**	**0.71**	**0.53**	**0.48**	**0.26**	**0.17**

GROUP 2	N	Sex	Age	Diagnosis	Initial	F/u 1	F/u 2	F/u 3	F/u 4
F/u years	1	M	70	PAF/DLB	0.0	2.0	3.9	6.3	8.7
^{18}F-DA	1				2151	1702	3231	3923	4498
^{18}F-DA Fx Initial	1				1.00	0.79	1.50	1.82	2.09
F/u years	2	M	63	PAF	0.0	6.0	11.0	13.6	15.7
^{18}F-DA	2				2184	3905	2532	3199	3390

^{18}F-DA Fx Initial	2				1.00	1.79	1.16	1.46	1.55
F/u years	3	F	67	PAF	0.0	2.3	4.0	6.2	8.2
^{18}F-DA	3				1948	3422	4157	2581	2594
^{18}F-DA Fx Initial	3				1.00	1.76	2.13	1.33	1.33
F/u years	4	M	58	PD	0.0	0.5	2.6	10.5	
^{18}F-DA	4				2096	No data	1830	868	
^{18}F-DA Fx Initial	4				1.00		0.87	0.41	
F/u years	5	F	72	PD/DLB	0.0	3.2	10.4		
^{18}F-DA	5				2344	2381	570		
^{18}F-DA Fx Initial	5				1.00	1.02	0.24		
F/u years	6	F	57	PAF	0.0	1.8	8.6		
^{18}F-DA	6				4830	3204	4212		
^{18}F-DA Fx Initial	6				1.00	0.66	0.87		
F/u years	7	M	62	PAF	0.0	1.1	9.6		
^{18}F-DA	7				5294	1990	3269		
^{18}F-DA Fx Initial	7				1.00	0.38	0.62		
F/u years	8	F	57	PAF/DLB/PD	0.0	1.9	3.0	4.4	6.1
^{18}F-DA	8				3194	3289	3472	3193	2346
^{18}F-DA Fx Initial	8				1.00	1.03	1.09	1.00	0.73
F/u years	9	F	66	PD	0.0	1.5	3.2	4.6	6.2
^{18}F-DA	9				5351	4546	5835	7133	7246
^{18}F-DA Fx Initial	9				1.00	0.85	1.09	1.33	1.35

F/u years					**0.0**	**2.3**	**6.3**	**7.6**	**9.0**
^{18}F-DA					**3266**	**3055**	**3234**	**3483**	**4015**
^{18}F-DA Fx Initial					**1.0**	**1.0**	**1.1**	**1.2**	**1.4**

In Group 1 (N=3) initial radioactivity was normal (above 6000 nCi-kg/cc-mCi) [54] and fell to below normal during follow-up. In Group 2 (N=9) initial radioactivity was subnormal (below 6000 nCi-kg/cc-mCi), with low radioactivity persisting during follow-up. Listed ages are in years. DLB=dementia with Lewy bodies; Dx=diagnosis; F=female; Fx Initial=fraction of initial value; M=male; PAF=pure autonomic failure; PD=Parkinson disease; PDRisk=multiple risk factors for PD, enrolled in the intramural NINDS PDRisk study. Diagnoses with slashes (/) indicate the temporal trends in symptoms.

Table S5. Post-mortem apical myocardial concentrations of catecholamines (norepinephrine (NE), dopamine (DA)) and in vivo interventricular septal myocardial ^{18}F-dopamine- (^{18}F-DA)-derived radioactivity in patients with Lewy body diseases (LBDs).

Patient	Sex	Age	Diagnosis	NE	DA	^{18}F-DA
LBD1	F	84	PD	0.036	0.0019	2526
LBD2	M	78	PD/DLB	0.432	0.0059	3729
LBD3	F	74	PAF	0.007	0.0000	1733
LBD4	M	69	PAF	0.034	0.0033	3218
LBD5	F	83	PD/DLB	0.048	0.0020	2381
LBD6	M	79	PAF/DLB/PD	0.019	0.0000	4498
Control	N=25	78		1.77	0.13	

Data are also shown from an ongoing database of age-matched control subjects who did not have LB pathology. Listed ages are in years. Catecholamine concentrations are in units of pmol/mg wet weight and ^{18}F-DA-derived radioactivity in units of nCi-kg/cc-mCi. Abbreviations: CON=control; DLB=dementia with Lewy bodies; F=female; M=male; PAF=pure autonomic failure. Diagnoses with slashes (/) indicate the temporal trends in symptoms. The LBD patients have drastically decreased myocardial NE and DA contents. All the patients had low ^{18}F-DA-derived radioactivity during life (normal $\geq$ 6000 nCi-kg/cc-mCi).[54]

Figure S1. Curves depicting (A) cerebrovascular autoregulation, (B) body temperature regulation, and (C) extracellular dopamine (DA) as a function of genetic variation in activities of the cell membrane DA transporter (DAT) and tyrosine hydroxylase (TH).

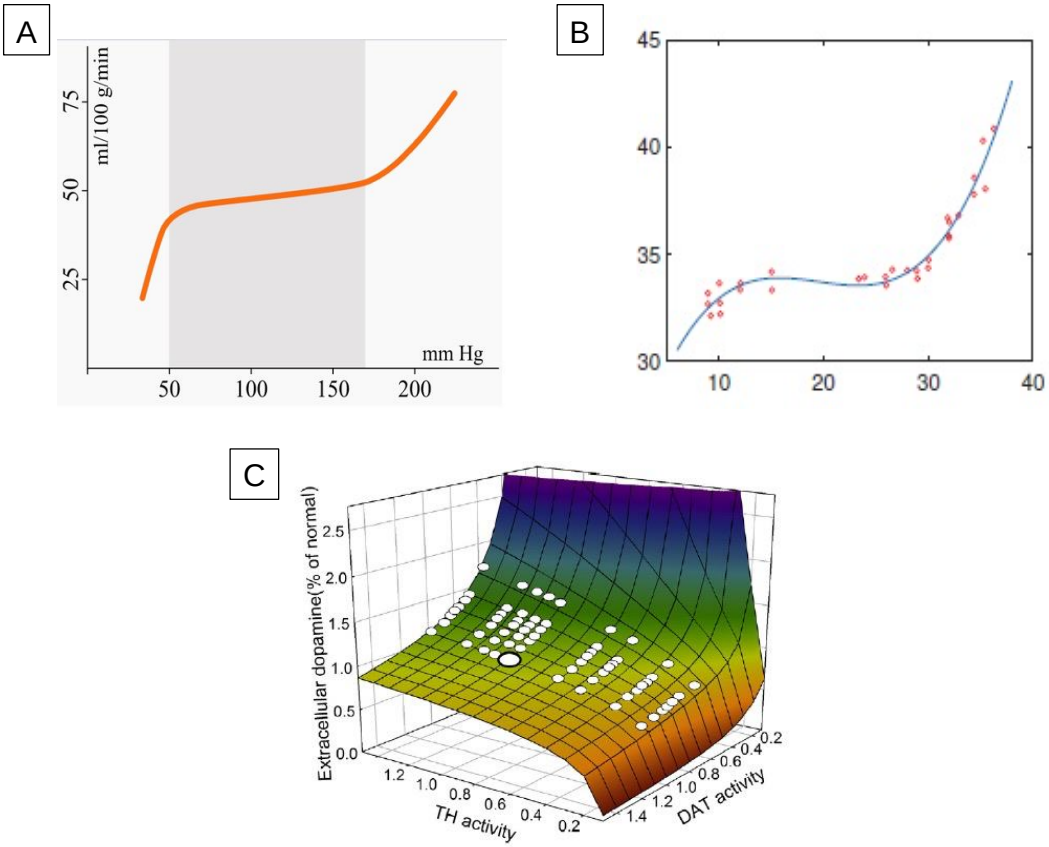

In (A), across a range of blood pressures (horizontal axis), cerebral blood flow (vertical axis) is kept within a relatively small range. At extremes of blood pressure, autoregulation breaks down (https://commons.wikimedia.org/wiki/File:Cerebrovascular_autoregulation.svg). In (B), body temperature of a brown opossum (vertical axis) is shown as a function of the ambient temperature (horizontal axis).[25, 57] (C) displays a homeostatic surface, where the state at the output node (in this case extracellular DA) is unaffected by changes in values for the two independent parameters TH and DAT activities.[24, 25] On this surface, the wild-type genotype is indicated by the large white circle. The smaller white circles indicate positions corresponding to genetic polymorphisms. All points on the surface are homeostatic. One can conceptualize the homeostatic surface changing as a result of accumulated stress (allostatic load). Dyshomeostasis would correspond to extracellular DA falling below the homeostatic surface. Panels B and C are reproduced from the Nijhout et al[25] with permission.

Figure S2. Pictorial representation of inhibitory (red) and stimulatory (green) effects of cytoplasmic DOPAL (DOPALc) on reactions in the computational model.

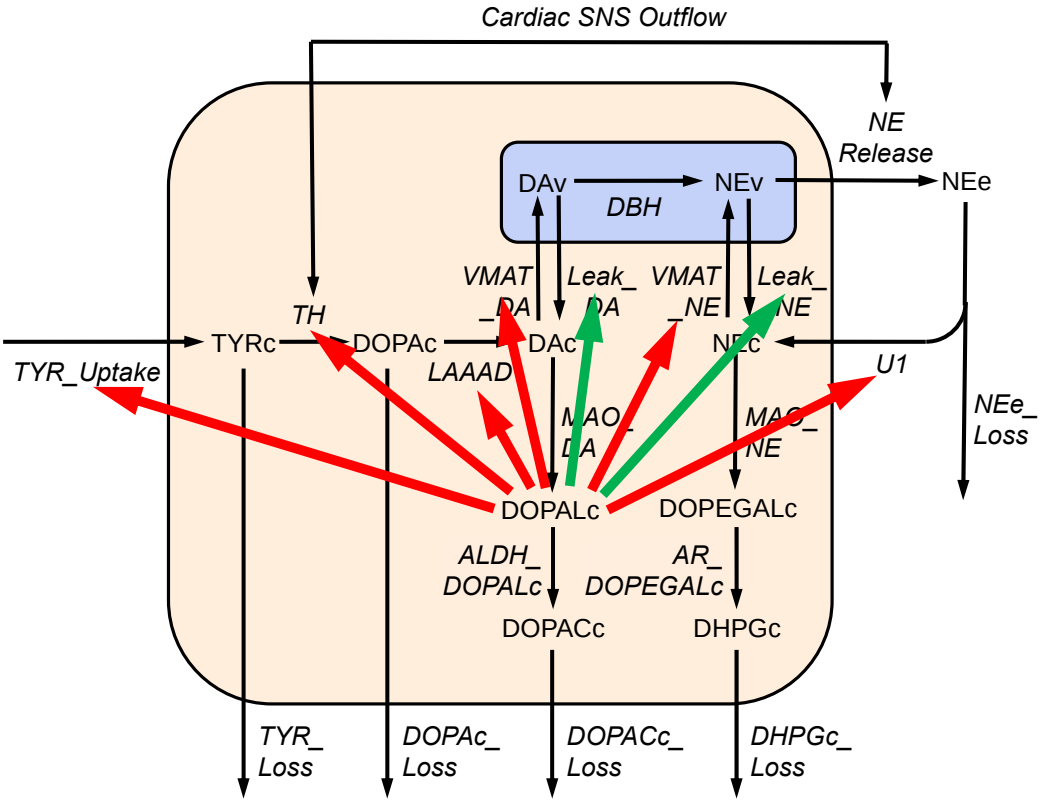

The model lumps effects of DOPAL, α-synuclein (αS), and DOPAL-αS interactions. For definitions of abbreviations see the legend for Figure 1.

Figure S3. Model-predicted effects of genetic variants on myocardial norepinephrine content (NEv).

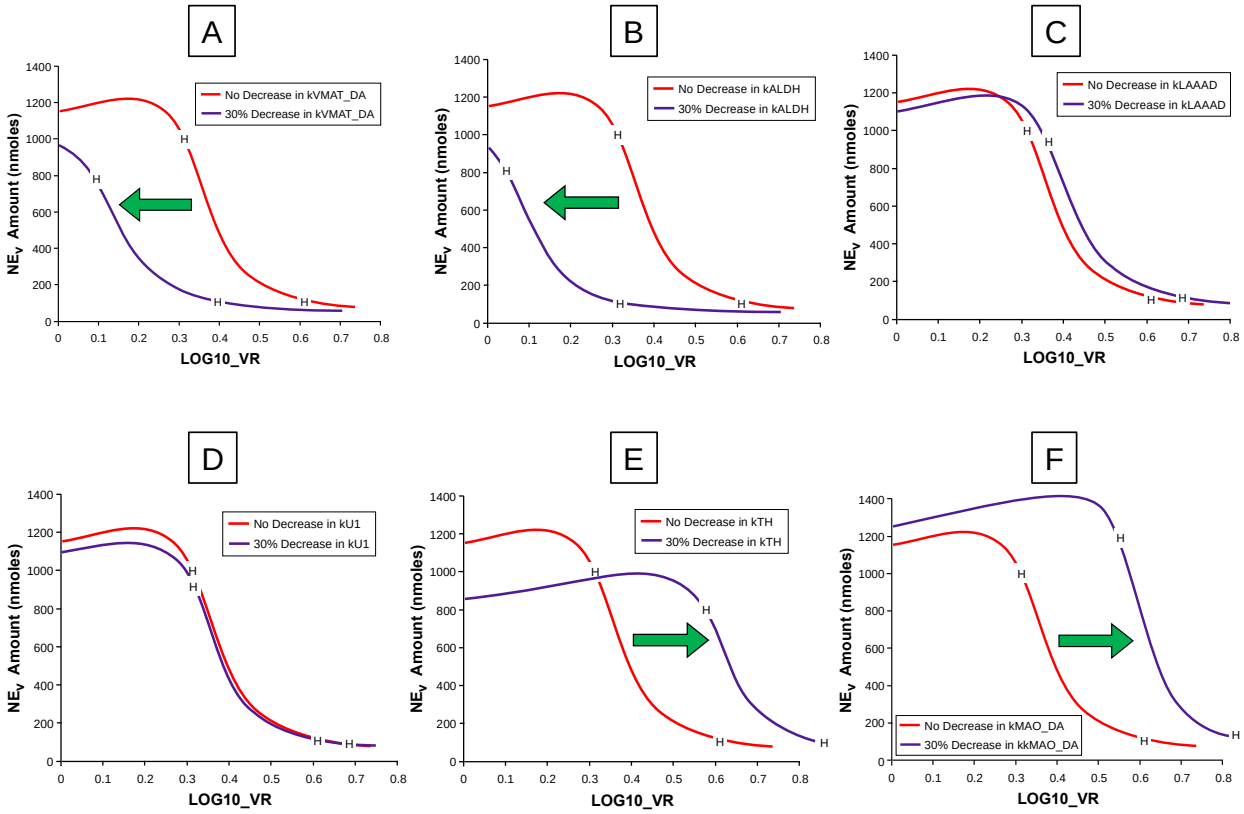

(A) 30% decrease in kVMAT_DA; (B) 30% decrease in kALDH; (C) 30% decrease in kLAAAD; (D) 30% decrease in kU1; (E) 30% decrease in kTH; (F) 30% decrease in kMAO_DA. In each panel the red curve indicates the relationship between NEv and the log of the vascular relaxation (Log10_VR), the stimulus for reflexively increased cardiac sympathetic outflow. H symbols indicate Hopf bifurcations. Green arrows indicate shifts in position of the curves for genetic variants (blue). The model predicts earlier Hopf bifurcations for 30% decreases in kVMAT_DA and kALDH and later Hopf bifurcations for 30% decreases in kTH and kMAO_DA.

Figure S4. Model-predicted effects of treatments on trends in cardiac norepinephrine stores (NEv).

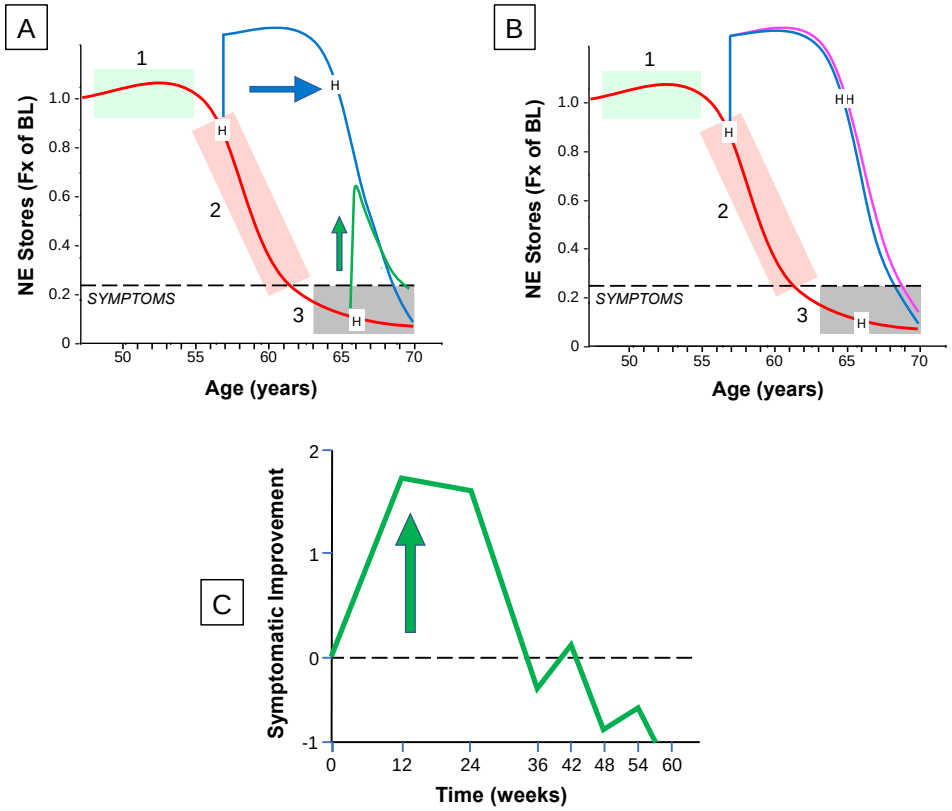

(A) Predicted effects of decreasing kMAO_DA by 30% beginning at the time of the first Hopf bifurcation, corresponding to the beginning of pre-symptomatic Phase 2 (blue) and the same decrease in kMAO_DA beginning at the time of the second Hopf bifurcation in symptomatic Phase 3 (green). (B) Predicted curve after decreasing kMAO_DA by 30% and decreasing by 30% the effects of DOPALc on kTYR_Uptake, kTH, kLAAAD, kVMAT_DA, kVMAT_NE, kU1, and kLeak at the time of the first Hopf bifurcation (magenta). Treatment decreasing kMAO_DA by 30% starting at the beginning of Phase 2 produces an immediate increase in NEv, shifts to the right the curve relating NEv vs. age (blue arrow), and delays the onset of symptomatic disease by about 7 years. The same treatment initiated in Phase 3 produces a smaller immediate increase in NEv and transiently alleviates symptoms, with symptoms recurring after about 4 years (green arrow). Additional treatment decreasing by 30% the effects of DOPALc on kTYR_Uptake, kTH, kLAAAD, kVMAT_DA, kVMAT_NE, kU1, and kLeak produces only a slight (about 1 year) delay in symptom onset. (C) Symptomatic improvement vs. duration of treatment with the MAO-B inhibitor rasagiline in PD (data derived from Olanow et al.[19]).